Numerical methods of chaos detection

Haris Skokos
Department of Mathematics and Applied Mathematics
University of Cape Town
Cape Town, South Africa

E-mail: haris.skokos@uct.ac.za – haris.skokos@gmail.com
URL: http://math_research.uct.ac.za/~hskokos/

20th Christmas Symposium of Physicists of the University of Maribor
14 December 2023, Maribor, Slovenia

University of Cape Town (UCT)

University of Cape Town (UCT)

Cape Town

Outline

- **Dynamical Systems**
  - ✓ **Hamiltonian models – Variational equations**
  - ✓ **Symplectic maps – Tangent map**

- **Brief presentation of chaos detection methods**

- **Chaos Indicators**
  - ✓ **Lyapunov exponents**
  - ✓ **Smaller ALignment Index – SALI**
    - **Definition**
    - **Behavior for chaotic and regular motion**
    - **Applications**
  - ✓ **Generalized ALignment Index – GALI**
    - **Definition - Relation to SALI**
    - **Behavior for chaotic and regular motion**
    - **Application to time-dependent models**

- **Chaos diagnostics based on Lagrangian descriptors (LDs)**

- **Summary**

Autonomous Hamiltonian systems

Consider an N degree of freedom autonomous Hamiltonian system having a Hamiltonian function of the form:

$$H(\overbrace{q_1,q_2,\ldots,q_N}^{\text{positions}}, \overbrace{p_1,p_2,\ldots,p_N}^{\text{momenta}})$$

The time evolution of an orbit (trajectory) with initial condition

$$P(0)=(q_1(0), q_2(0),\ldots,q_N(0), p_1(0), p_2(0),\ldots,p_N(0))$$

is governed by the Hamilton's equations of motion

$$\frac{dp_i}{dt} = -\frac{\partial H}{\partial q_i} \quad , \qquad \frac{dq_i}{dt} = \frac{\partial H}{\partial p_i}$$

Variational Equations

We use the notation $\mathbf{x} = (q_1,q_2,\ldots,q_N,p_1,p_2,\ldots,p_N)^T$. The deviation vector from a given orbit is denoted by

$$\mathbf{v} = (\delta x_1, \delta x_2,\ldots,\delta x_n)^T \text{, with } n=2N$$

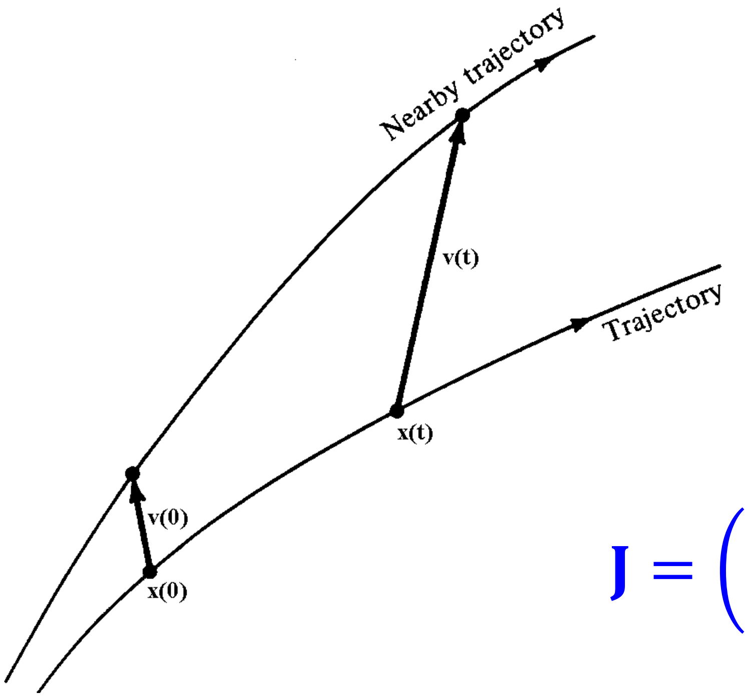

Benettin & Galgani, 1979, in Laval and Gressillon (eds.), op cit, 93

The time evolution of v is given by the so-called variational equations:

$$\frac{d\mathbf{v}}{dt} = -\mathbf{J}\cdot\mathbf{P}\cdot\ \mathbf{v}$$

where

$$\mathbf{J} = \begin{pmatrix} 0_N & -I_N \\ I_N & 0_N \end{pmatrix}, P_{ij} = \frac{\partial^2 H}{\partial x_i \partial x_j} \quad i,j = 1,2,\ldots,n$$

Symplectic Maps

Consider an 2N-dimensional symplectic map T. In this case we have discrete time.

The evolution of an orbit with initial condition

$$P(0)=(x_1(0), x_2(0),\ldots,x_{2N}(0))$$

is governed by the equations of map T

$$P(i+1)=T\,P(i)\;\;,\;\; i=0,1,2,\ldots$$

The evolution of an initial deviation vector

$$v(0) = (\delta x_1(0), \delta x_2(0),\ldots, \delta x_{2N}(0))$$

is given by the corresponding tangent map

$$v(i+1) = \left.\frac{\partial T}{\partial P}\right|_i \cdot v(i)\;\;, i = 0, 1, 2, \ldots$$

Chaos detection techniques

- **Based on the visualization of orbits**
  - ✓ **Poincaré Surface of Section (PSS)**
  - ✓ **the color and rotation (CR) method**
  - ✓ **the 3D phase space slices (3PSS) technique**

Poincaré Surface of Section (PSS)

We can constrain the study of an N+1 degree of freedom Hamiltonian system to a 2N-dimensional subspace of the general phase space.

In this sense an N+1 degree of freedom Hamiltonian system corresponds to a 2N-dimensional symplectic map.

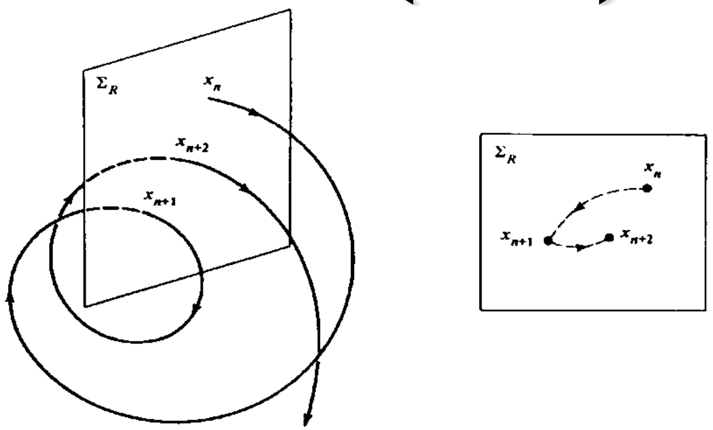

Lieberman & Lichtenberg, 1992, *Regular and Chaotic Dynamics*, Springer.

The 2D Hénon-Heiles system:

$$H_2 = \frac{1}{2}(p_x^2 + p_y^2) + \frac{1}{2}(x^2 + y^2) + x^2 y - \frac{1}{3}y^3$$

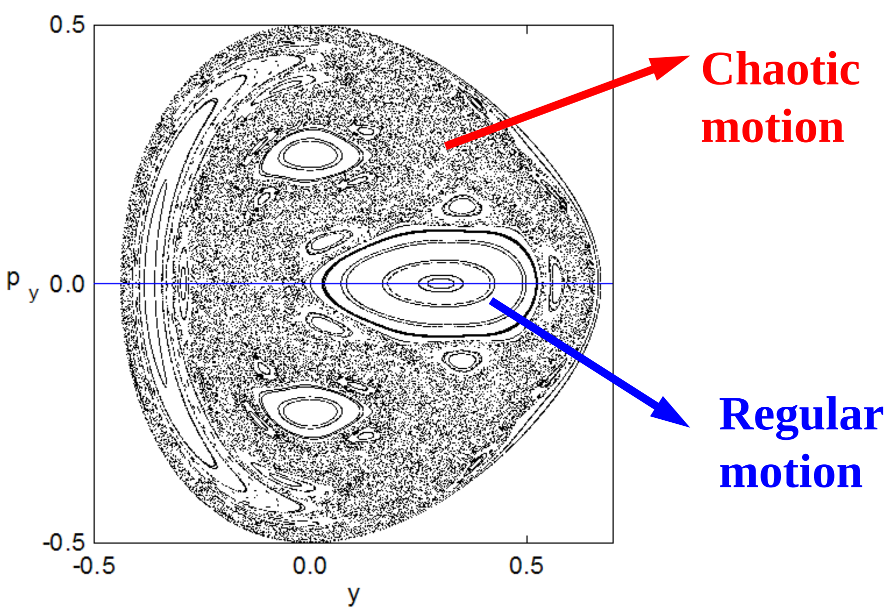

The color and rotation (CR) method

For 3 degree of freedom Hamiltonian systems and 4 dimensional symplectic maps:

We consider the 3D projection of the PSS and use color to indicate the 4th dimension.

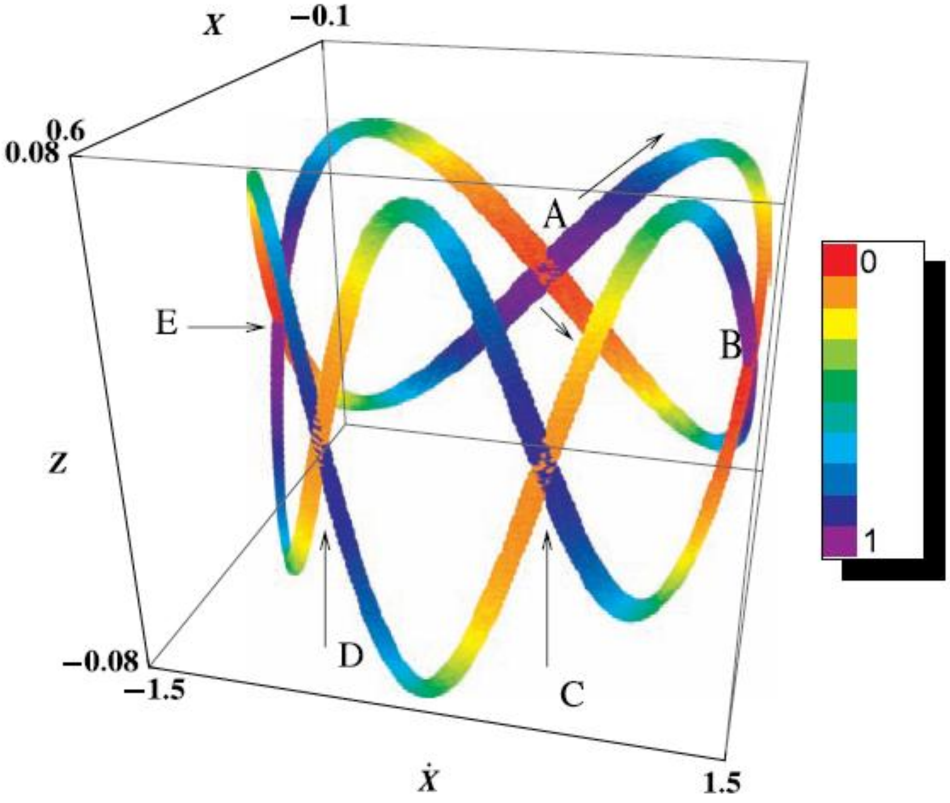

Katsanikas & Patsis, Int. J. Bif. Chaos (2011)

The 3D phase space slices (3PSS) technique

For 3 degree of freedom Hamiltonian systems and 4 dimensional symplectic maps:

We consider thin 3D phase space slices of the 4D phase space (e.g. $|p_2| \leq \varepsilon$) and present intersections of orbits with these slices.

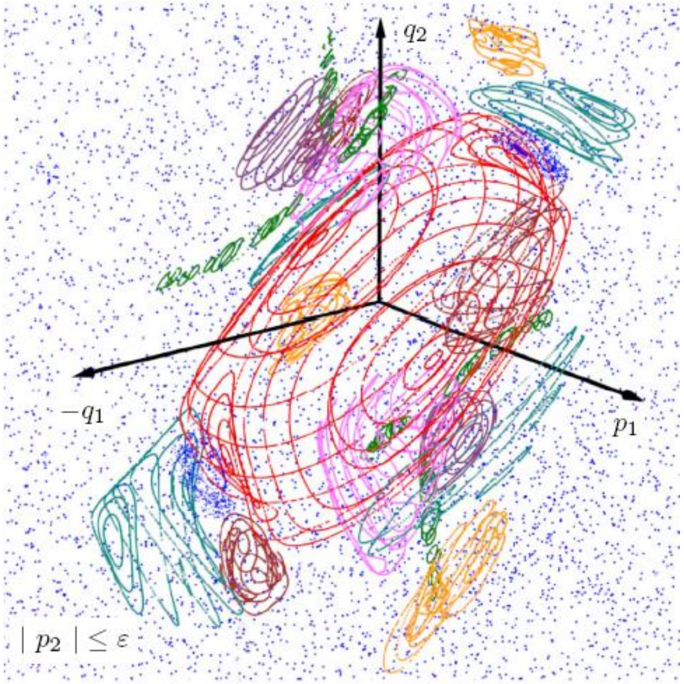

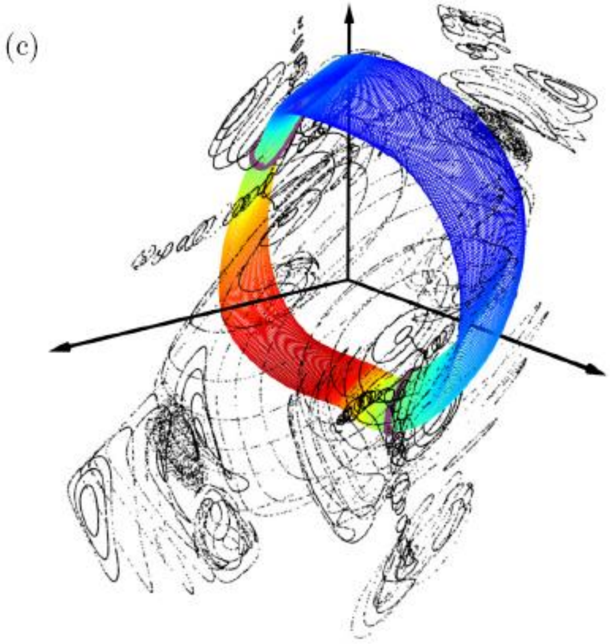

Richter et al., Phys. Rev. E (2014)

Chaos detection techniques

- **Based on the visualization of orbits**
  - ✓ **Poincaré Surface of Section (PSS)**
  - ✓ **the color and rotation (CR) method**
  - ✓ **the 3D phase space slices (3PSS) technique**
- **Based on the numerical analysis of orbits**
  - ✓ **Frequency Map Analysis**
  - ✓ **0-1 test**

Frequency Map Analysis

Create Frequency Maps by computing the fundamental frequencies of orbits.

Regular motion: The computed frequencies do not vary in time

Chaotic motion: The computed frequencies vary in time

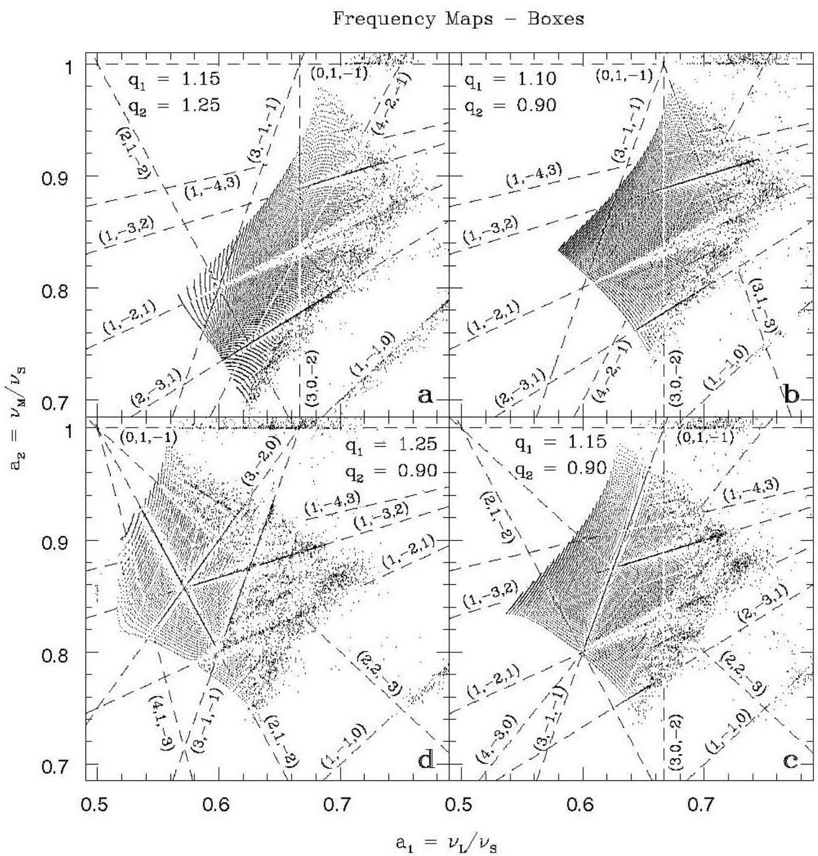

Papaphilippou & Laskar, Astron. Astrophys. (1998)

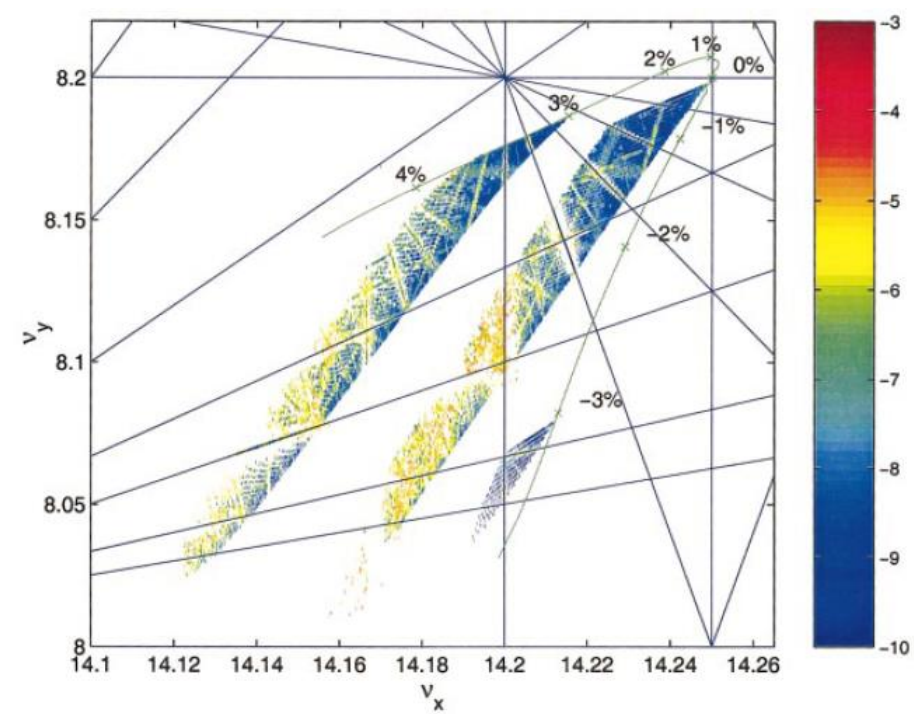

Steier et al., Phys. Rev. E (2002)

Frequency Map Analysis

Stability of Trojan asteroids, (α, e) diagram [Robutel & Gabern, MNRAS (2006)]

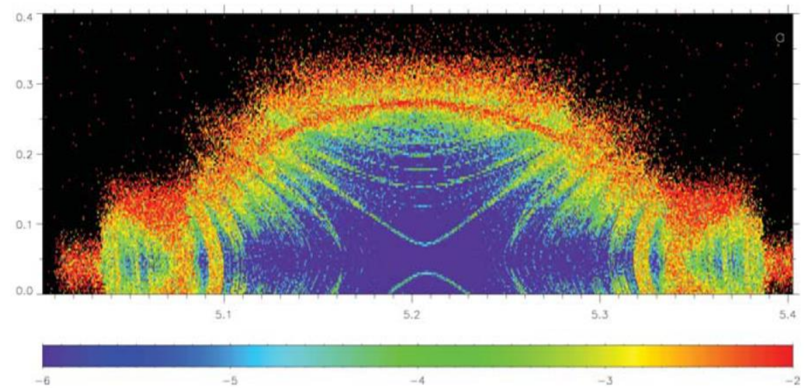

Dynamics of the European Synchrotron Radiation Facility (ESRF) storage ring [S. et al., 2004, in Proc. of the 9th European Particle Accelerator Conf. (EPAC)]

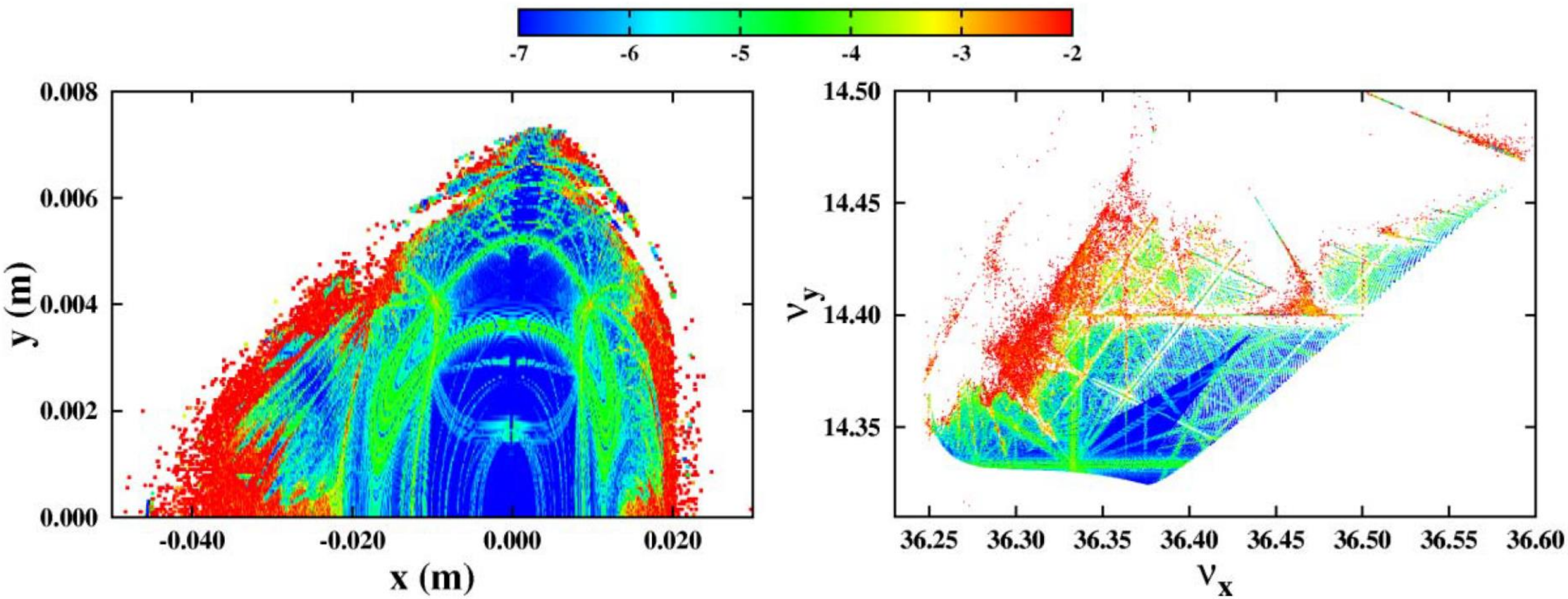

Chaos detection techniques

- **Based on the visualization of orbits**
  - ✓ **Poincaré Surface of Section (PSS)**
  - ✓ **the color and rotation (CR) method**
  - ✓ **the 3D phase space slices (3PSS) technique**
- **Based on the numerical analysis of orbits**
  - ✓ **Frequency Map Analysis**
  - ✓ **0-1 test**
- **Chaos indicators based on the evolution of deviation vectors from a given orbit**
  - ✓ **Maximum Lyapunov Exponent (MLE)**
  - ✓ **Fast Lyapunov Indicator (FLI) and Orthogonal Fast Lyapunov Indicators (OFLI and OFLI2)**
  - ✓ **Mean Exponential Growth Factor of Nearby Orbits (MEGNO)**
  - ✓ **Relative Lyapunov Indicator (RLI)**
  - ✓ **Smaller ALignment Index – SALI**
  - ✓ **Generalized ALignment Index – GALI**

Maximum Lyapunov Exponent (MLE)

Chaos: sensitive dependence on initial conditions.

Roughly speaking, the MLE of a given orbit characterizes the mean exponential rate of divergence of trajectories surrounding it.

Consider an orbit in the 2N-dimensional phase space with initial condition x(0) and an initial deviation vector (small perturbation) from it v(0).
Then the mean exponential rate of divergence is:

$$\text{MLE}=\lambda_1 = \lim_{t\to\infty} \Lambda(t) = \lim_{t\to\infty} \frac{1}{t} \ln \frac{\|v(t)\|}{\|v(0)\|}$$

$\lambda_1=0 \rightarrow$ **Regular motion** ($\Lambda \propto t^{-1}$)

$\lambda_1>0 \rightarrow$ **Chaotic motion**

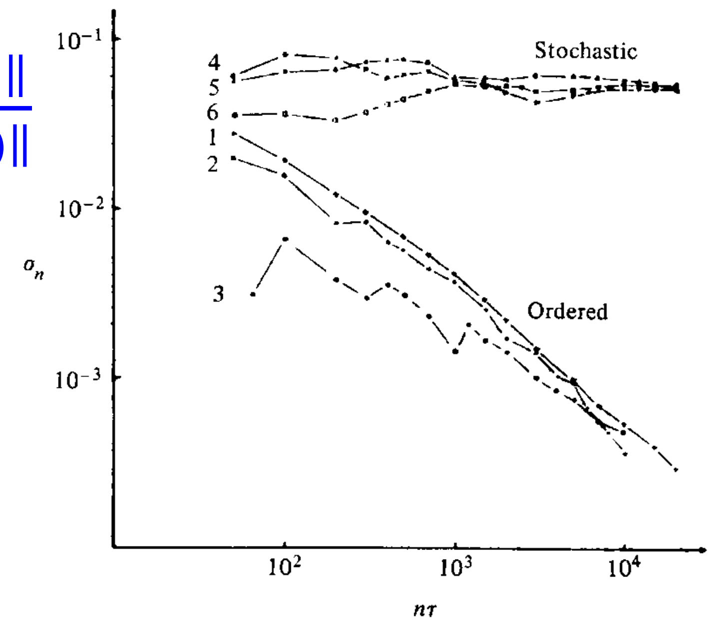

Figure 5.7. Behavior of σ_n at the intermediate energy $E = 0.125$ for initial points taken in the ordered (curves 1–3) or stochastic (curves 4–6) regions (after Benettin *et al.*, 1976).

The
Smaller ALignment Index
(SALI)
method

Definition of the SALI

We follow the evolution in time of two different initial deviation vectors ($v_1(0)$, $v_2(0)$), and define SALI [S., J. Phys. A (2001) – S. & Manos, Lect. Notes Phys. (2016)] as:

$$\mathbf{SALI(t) = min\{\|\hat{v}_1(t) + \hat{v}_2(t)\|, \|\hat{v}_1(t) - \hat{v}_2(t)\|\}}$$

where

$$\hat{\mathbf{v}}_1(\mathbf{t}) = \frac{\mathbf{v}_1(\mathbf{t})}{\|\mathbf{v}_1(\mathbf{t})\|}$$

When the two vectors become collinear

$$\mathbf{SALI(t) \rightarrow 0}$$

Behavior of SALI for chaotic motion

For chaotic orbits the two initially different deviation vectors tend to coincide with the direction defined by the maximum Lyapunov exponent.

Behavior of SALI for chaotic motion

For chaotic orbits the two initially different deviation vectors tend to coincide with the direction defined by the maximum Lyapunov exponent.

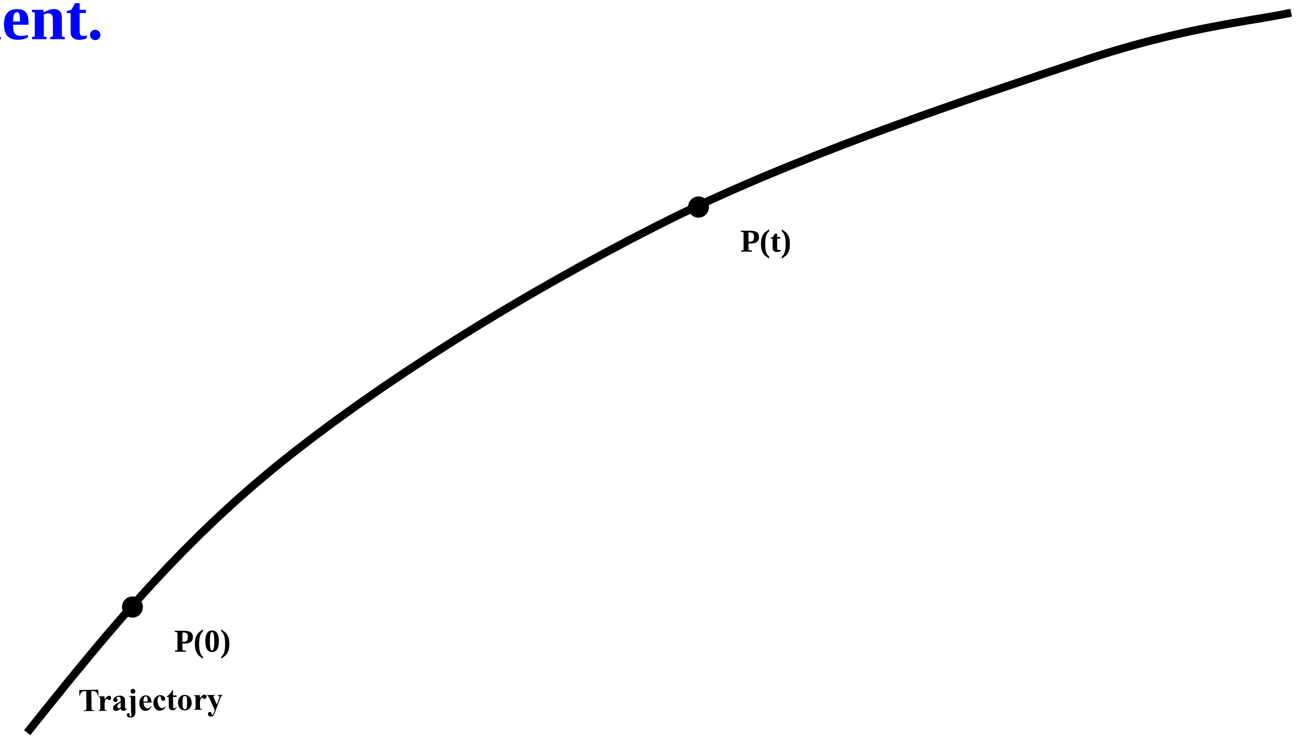

Behavior of SALI for chaotic motion

For chaotic orbits the two initially different deviation vectors tend to coincide with the direction defined by the maximum Lyapunov exponent.

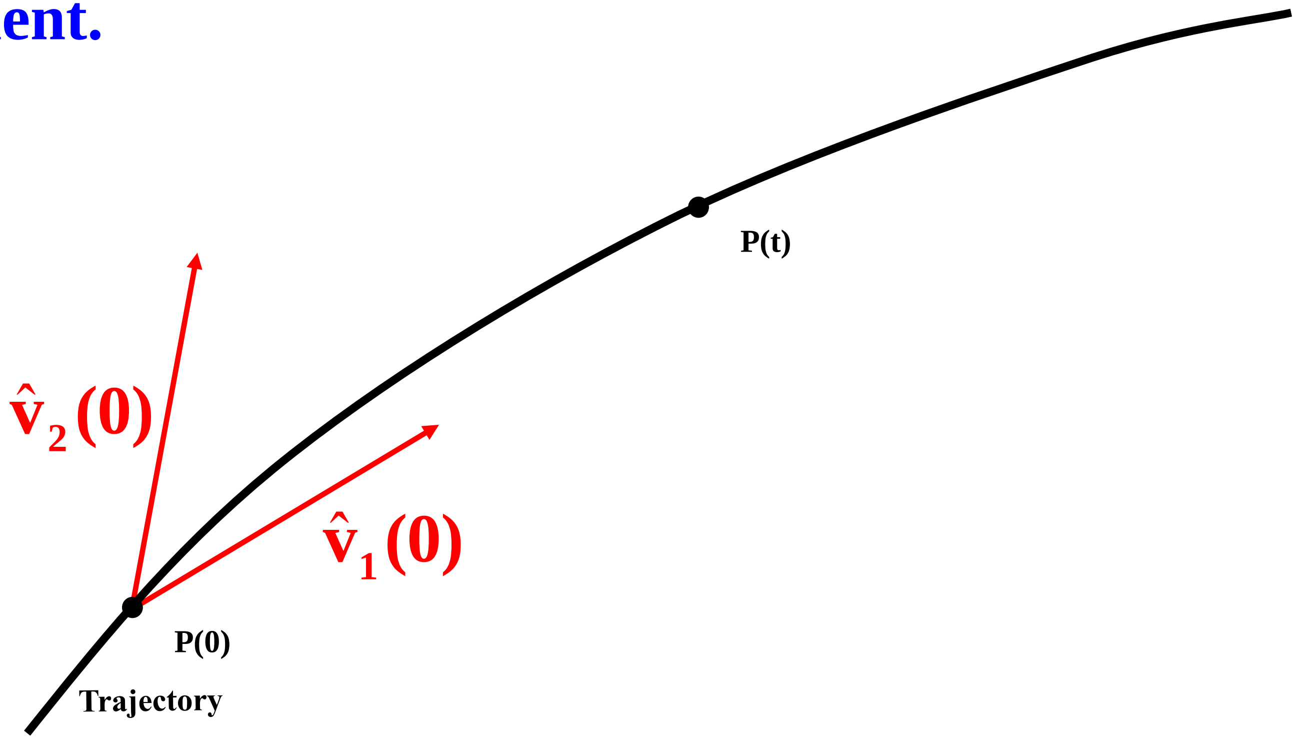

Behavior of SALI for chaotic motion

For chaotic orbits the two initially different deviation vectors tend to coincide with the direction defined by the maximum Lyapunov exponent.

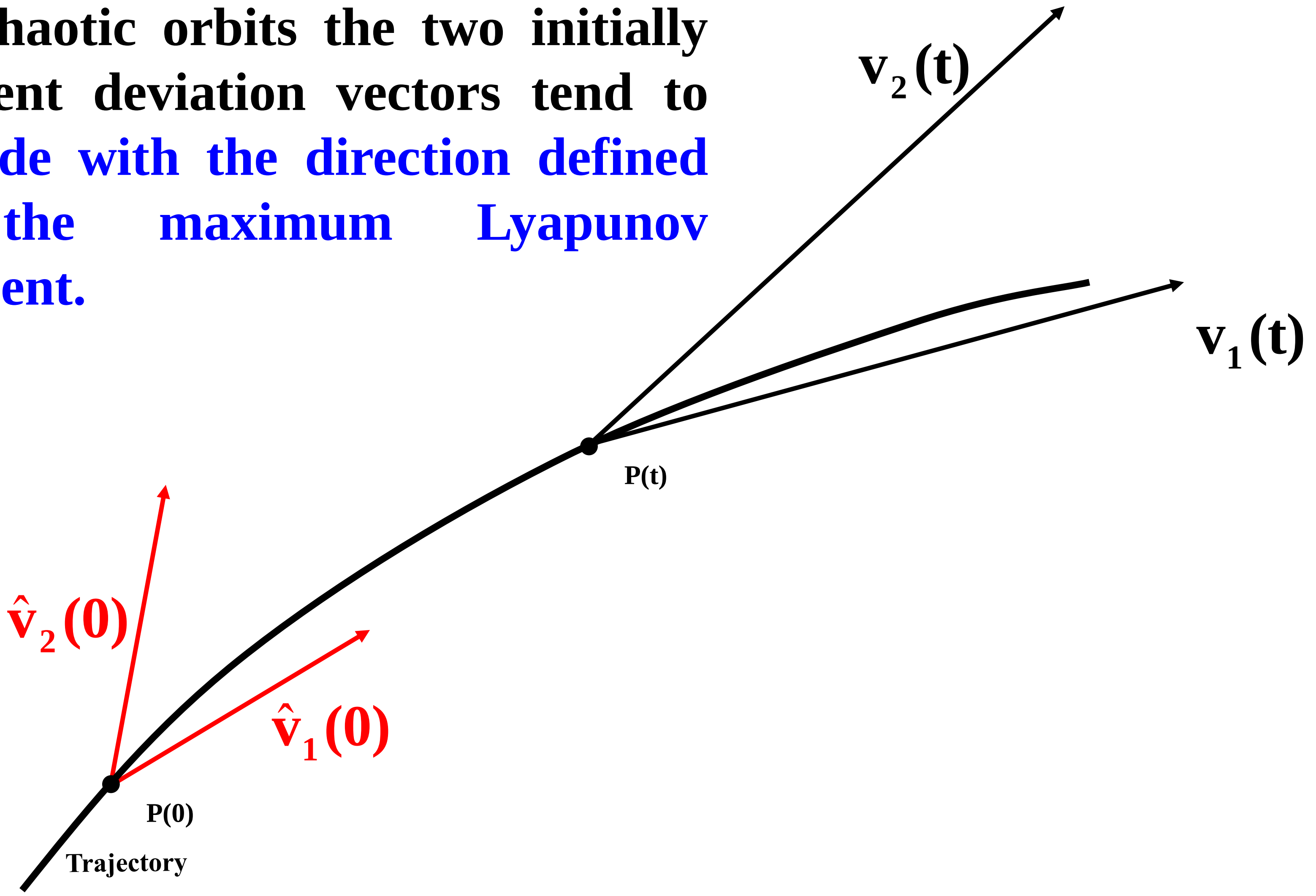

Behavior of SALI for chaotic motion

For chaotic orbits the two initially different deviation vectors tend to coincide with the direction defined by the maximum Lyapunov exponent.

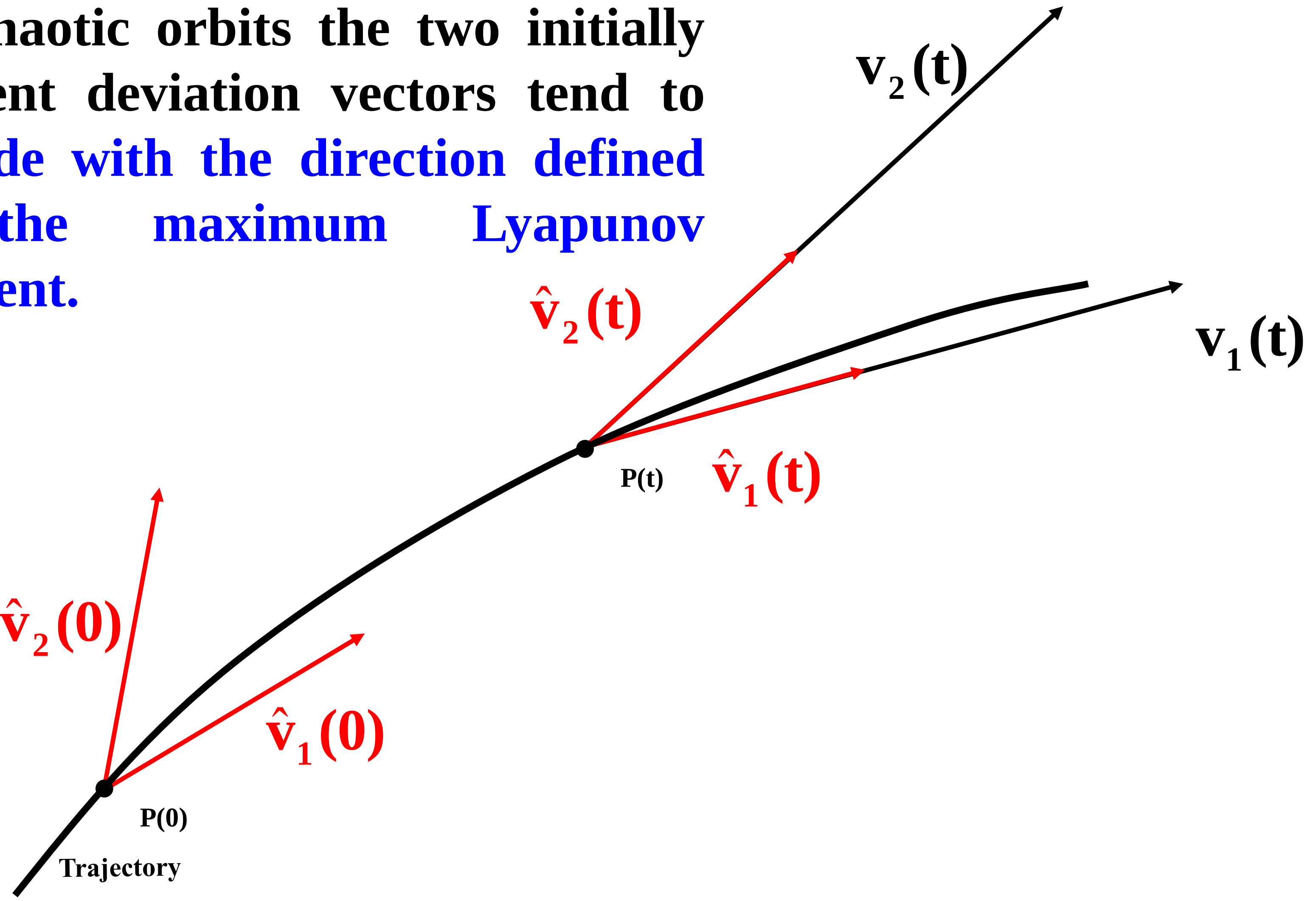

Behavior of SALI for chaotic motion

For chaotic orbits the two initially different deviation vectors tend to coincide with the direction defined by the maximum Lyapunov exponent.

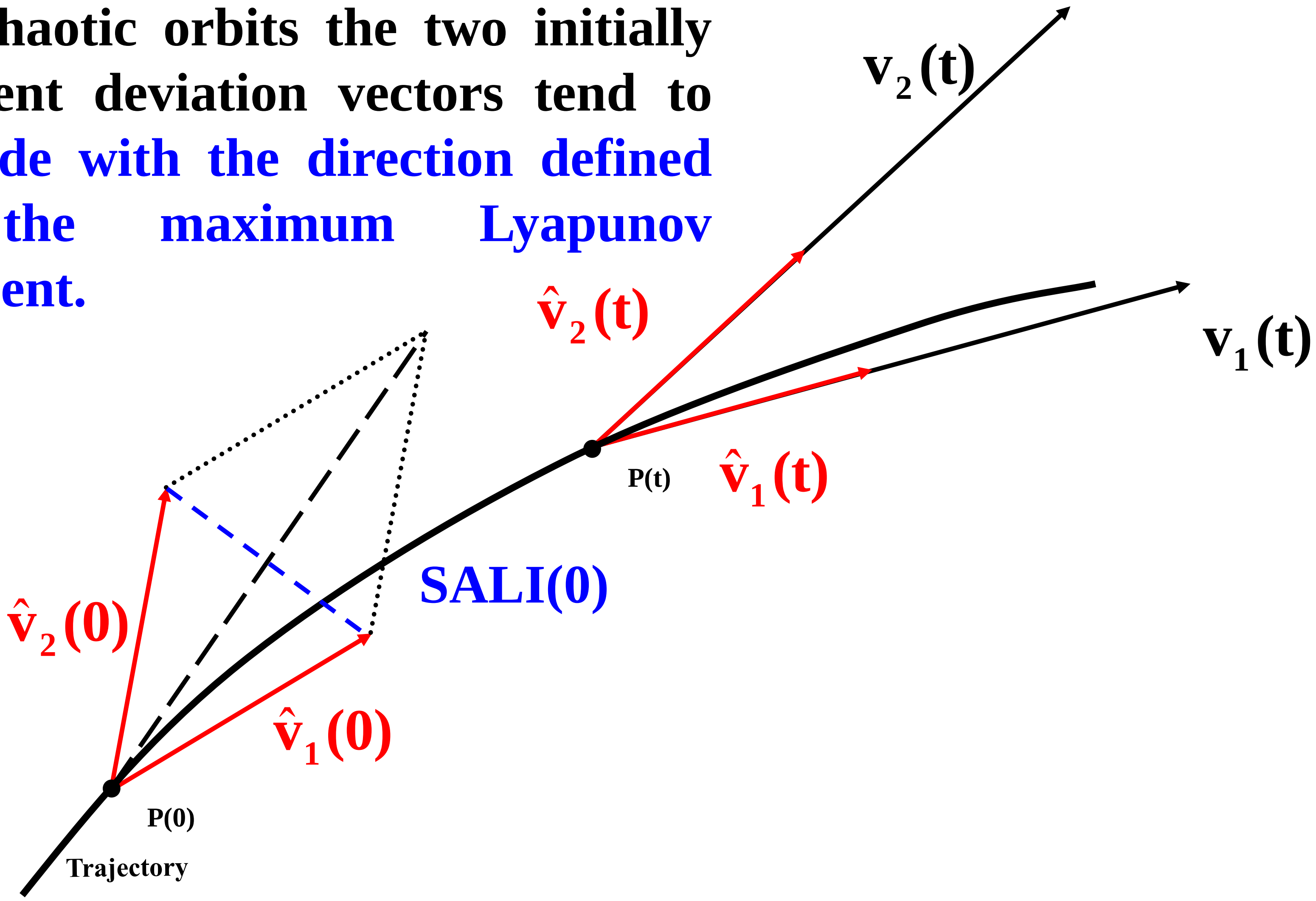

Behavior of SALI for chaotic motion

For chaotic orbits the two initially different deviation vectors tend to coincide with the direction defined by the maximum Lyapunov exponent.

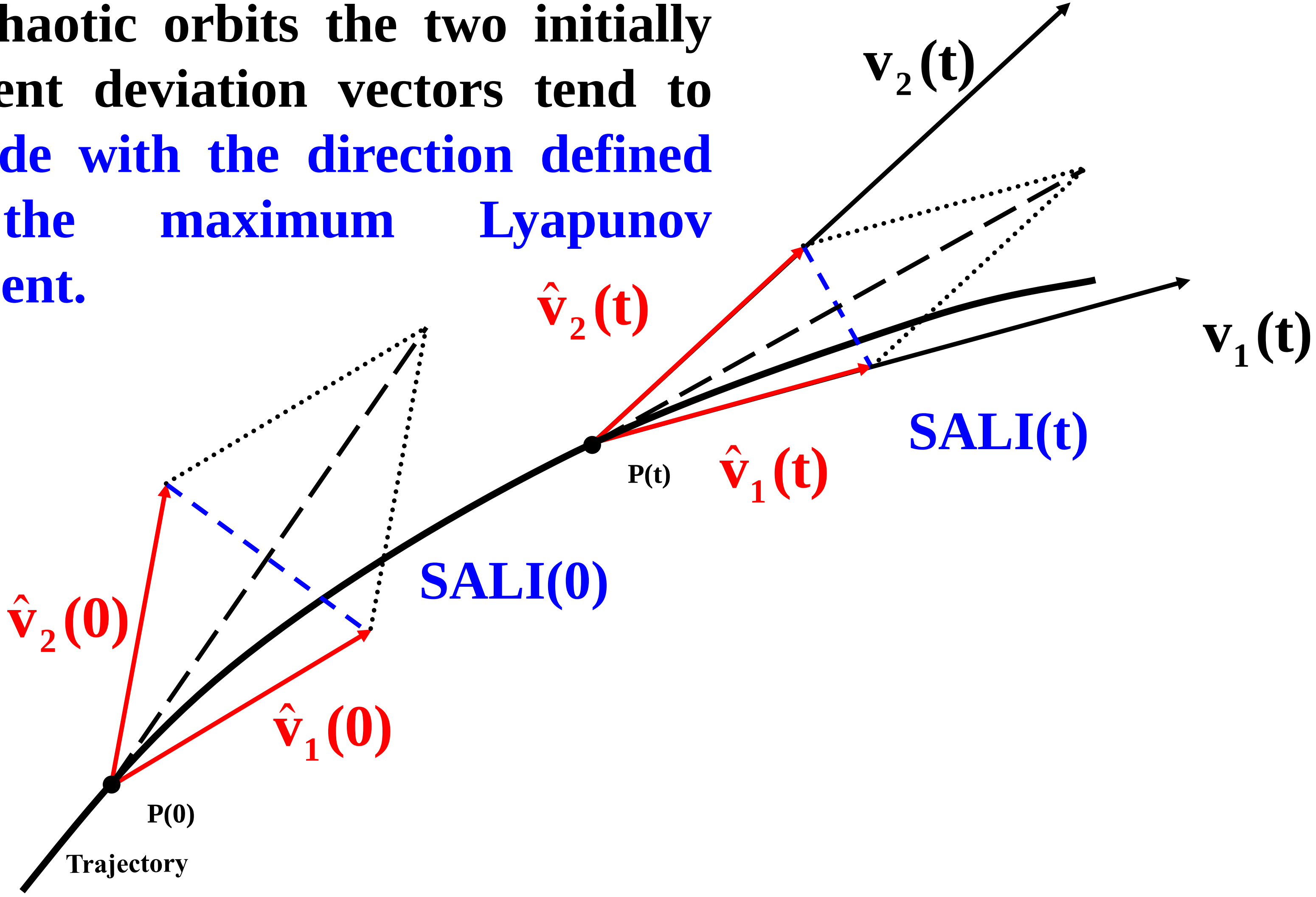

Behavior of the SALI for chaotic motion

We test the validity of the approximation $\boxed{\text{SALI} \propto e^{-(\lambda_1-\lambda_2)t}}$ [S. et al., J. Phys. A (2004)] for a chaotic orbit of the 3D Hamiltonian

$$H = \sum_{i=1}^{3} \frac{\omega_i}{2}(q_i^2 + p_i^2) + q_1^2 q_2 + q_1^2 q_3$$

with ω_1=1, ω_2=1.4142, ω_3=1.7321, H=0.09

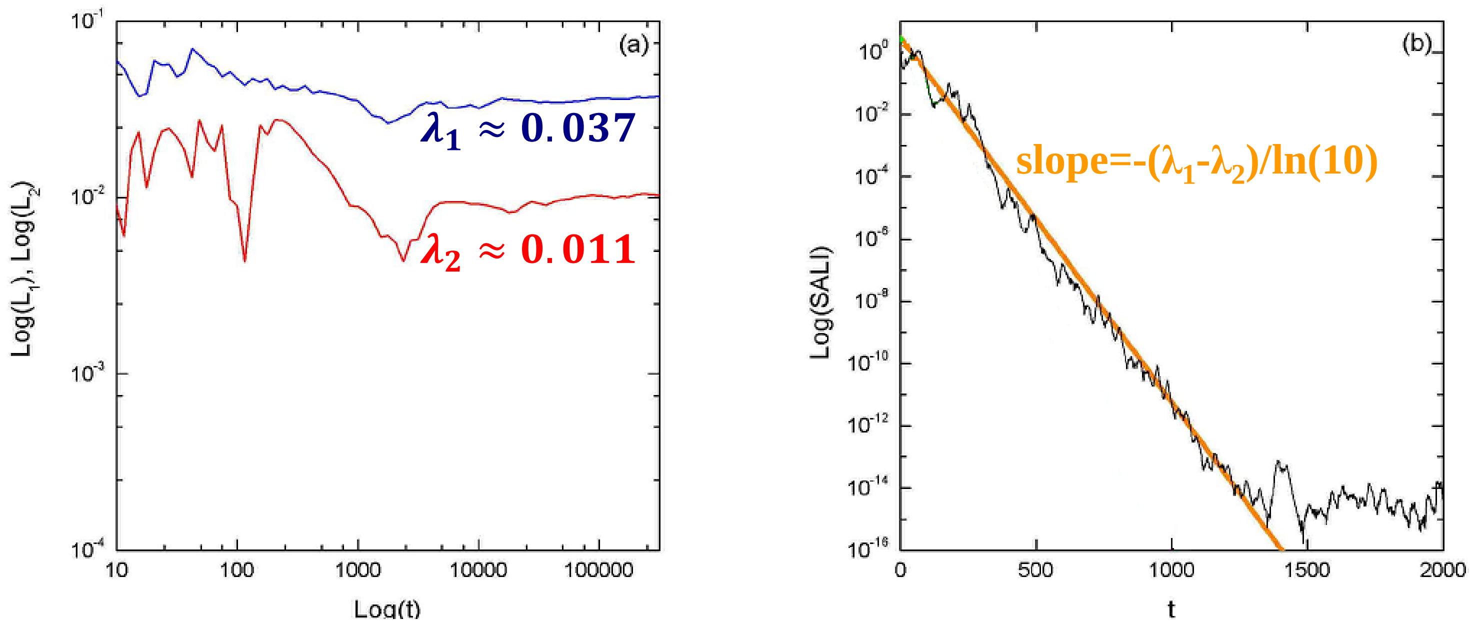

Behavior of SALI for regular motion

Regular motion occurs on a torus and two different initial deviation vectors become tangent to the torus, generally having different directions.

Behavior of SALI for regular motion

Regular motion occurs on a torus and two different initial deviation vectors become tangent to the torus, generally having different directions.

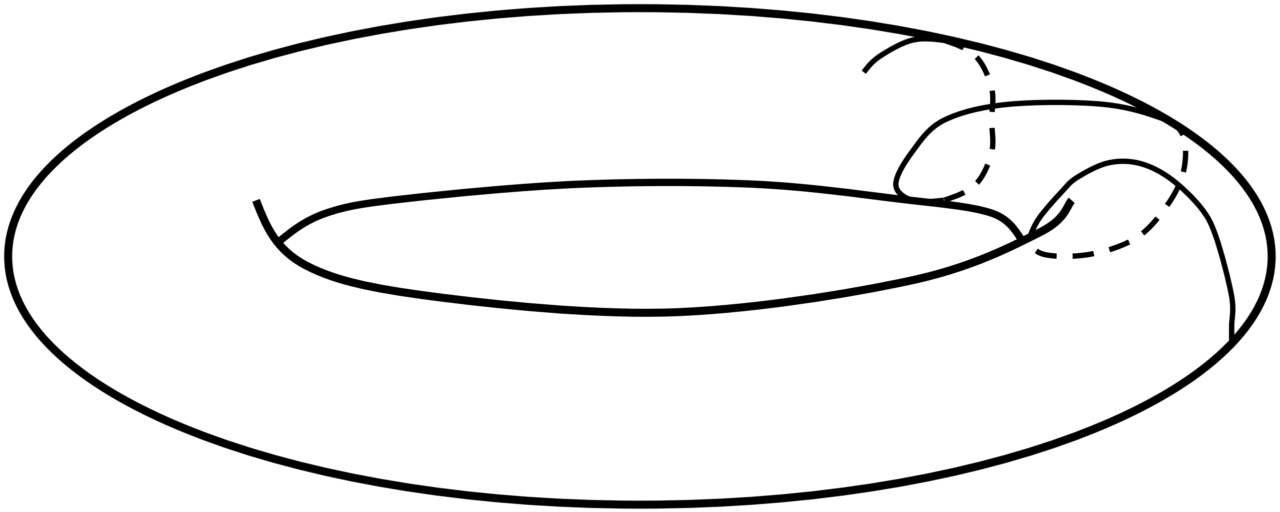

Behavior of SALI for regular motion

Regular motion occurs on a torus and two different initial deviation vectors become tangent to the torus, generally having different directions.

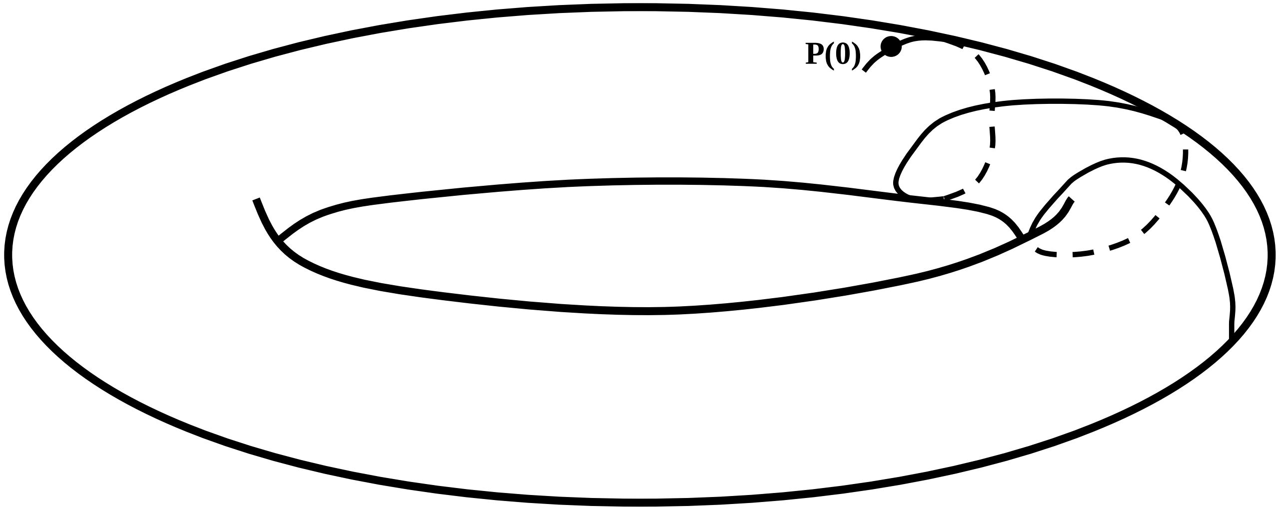

Behavior of SALI for regular motion

Regular motion occurs on a torus and two different initial deviation vectors become tangent to the torus, generally having different directions.

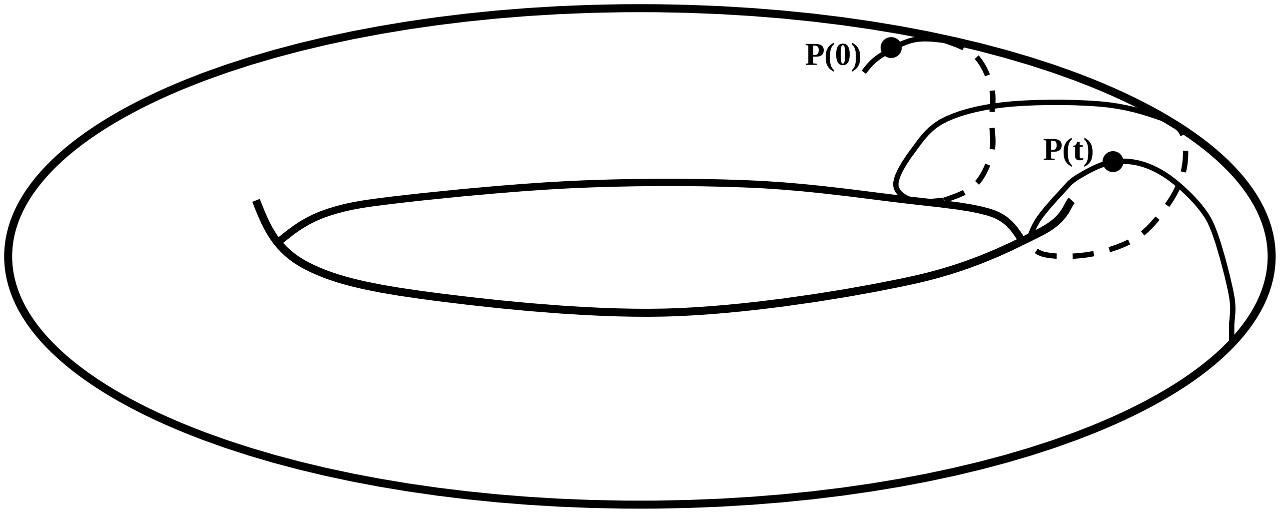

Behavior of SALI for regular motion

Regular motion occurs on a torus and two different initial deviation vectors become tangent to the torus, generally having different directions.

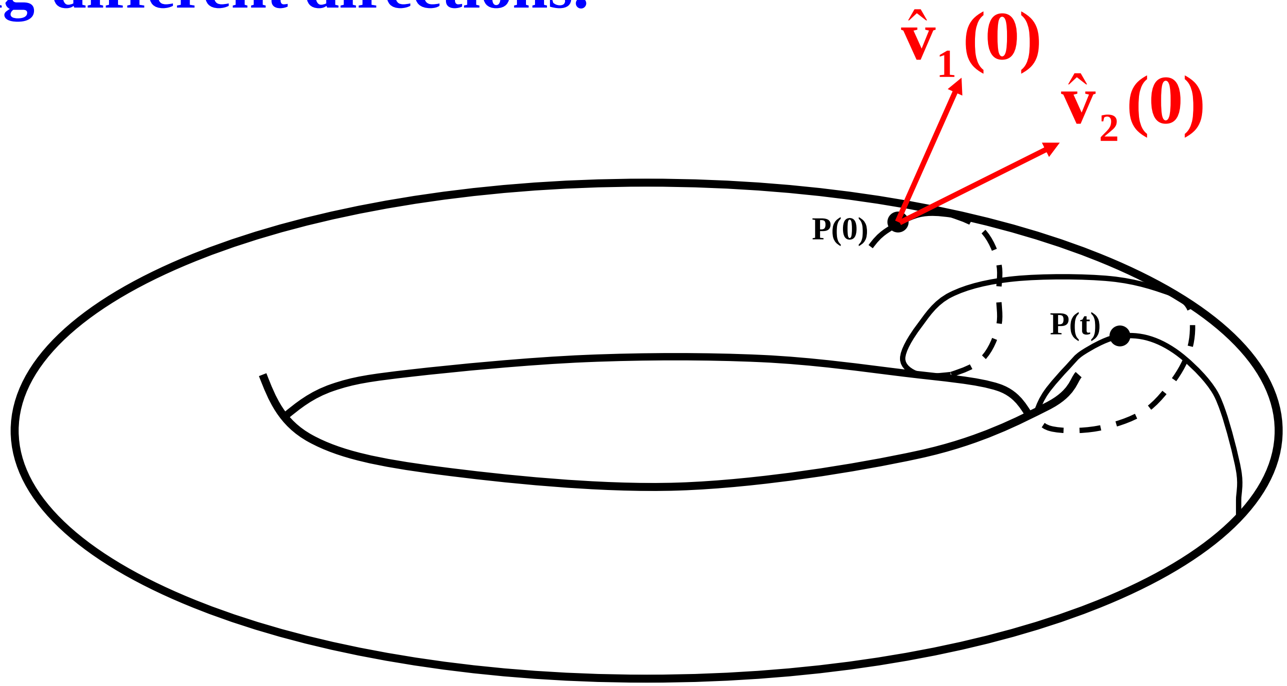

Behavior of SALI for regular motion

Regular motion occurs on a torus and two different initial deviation vectors become tangent to the torus, generally having different directions.

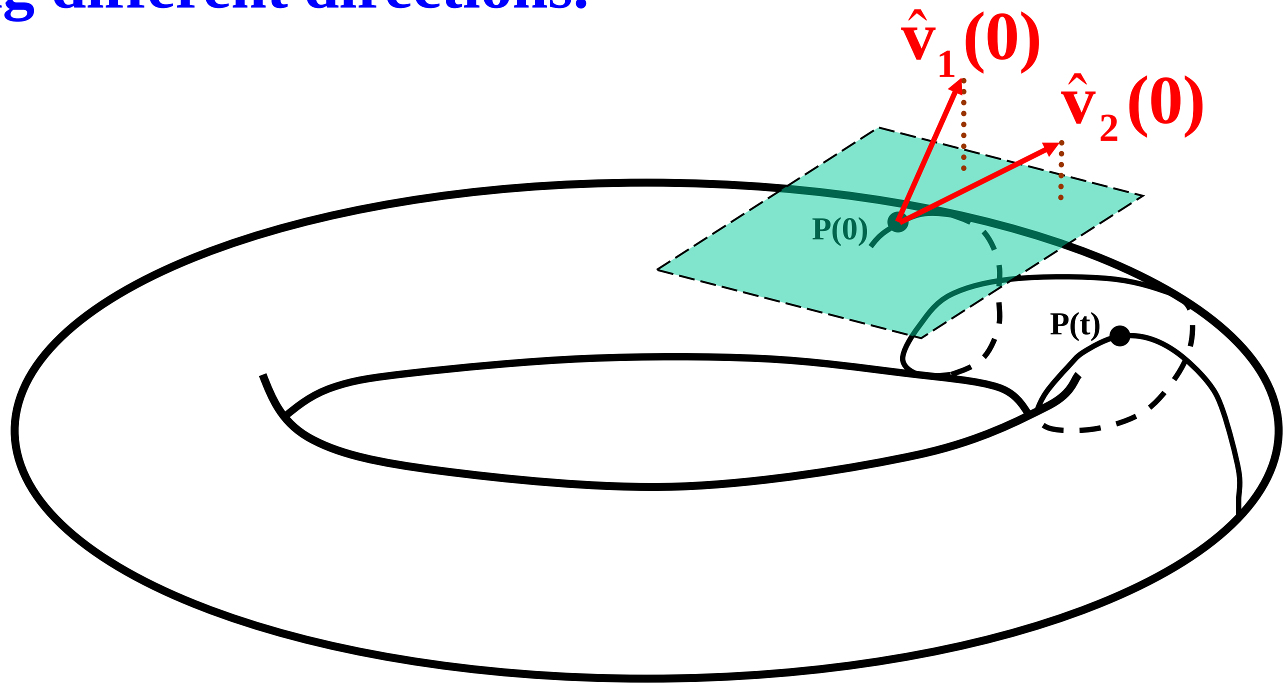

Behavior of SALI for regular motion

Regular motion occurs on a torus and two different initial deviation vectors become tangent to the torus, generally having different directions.

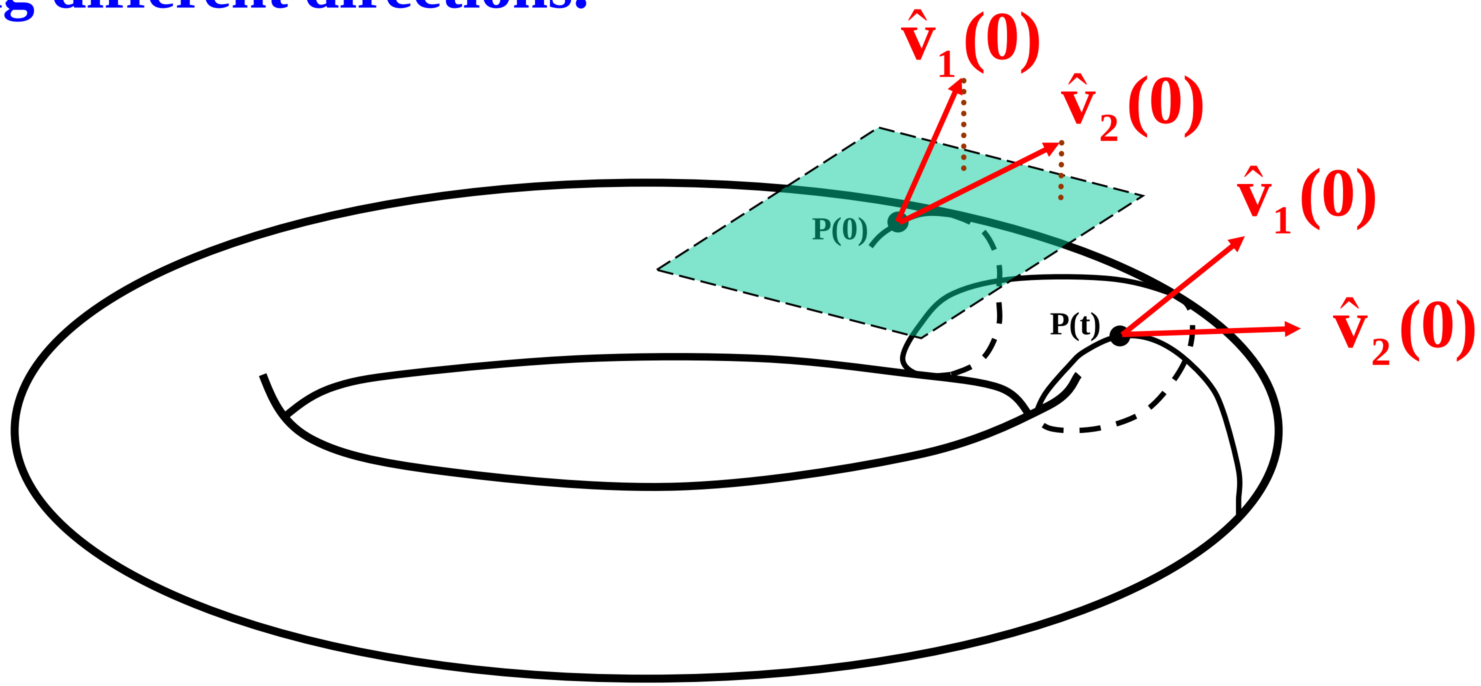

Behavior of SALI for regular motion

Regular motion occurs on a torus and two different initial deviation vectors become tangent to the torus, generally having different directions.

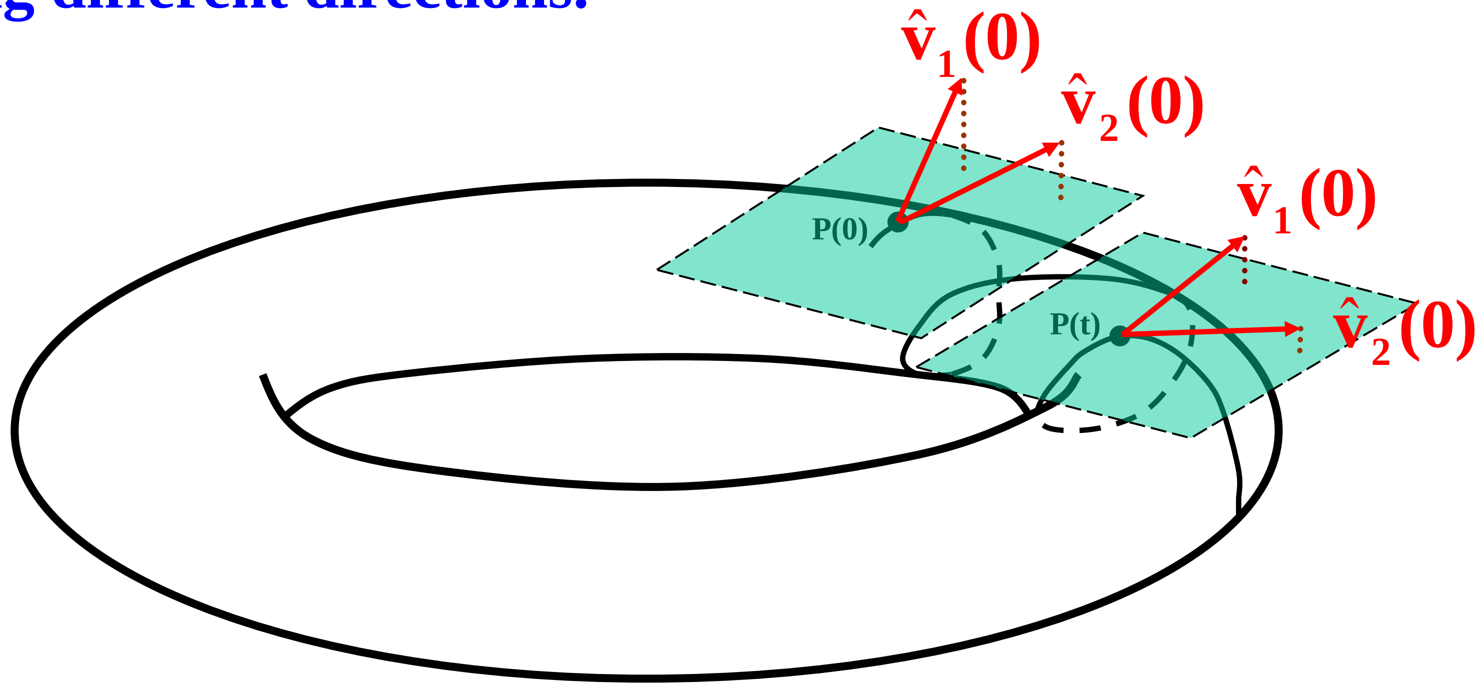

SALI – Hénon-Heiles system

As an example, we consider the 2D Hénon-Heiles system:

$$H = \frac{1}{2}\left(p_x^2 + p_y^2\right) + \frac{1}{2}\left(x^2 + y^2\right) + x^2 y - \frac{1}{3} y^3$$

For E=1/8 we consider the orbits with initial conditions:
Regular orbit, x=0, y=0.55, p_x=0.2417, p_y=0
Chaotic orbit, x=0, y=-0.016, p_x=0.49974, p_y=0
Chaotic orbit, x=0, y=-0.01344, p_x=0.49982, p_y=0

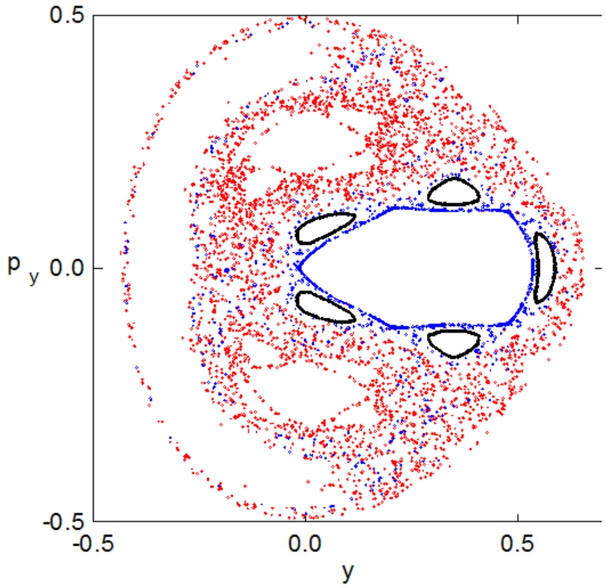

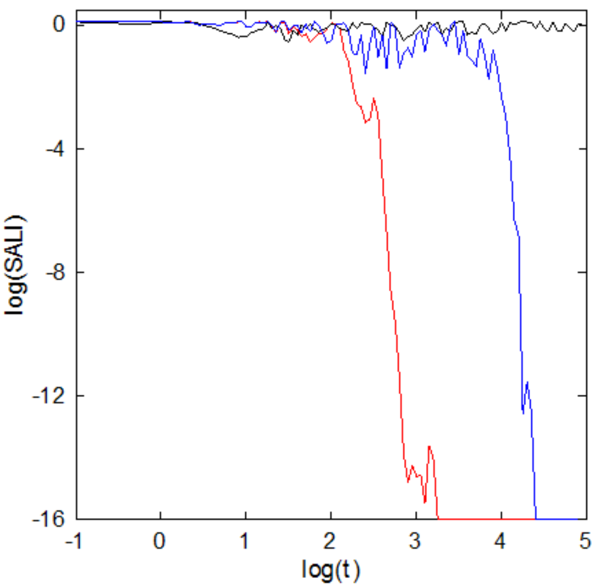

SALI – Hénon-Heiles system

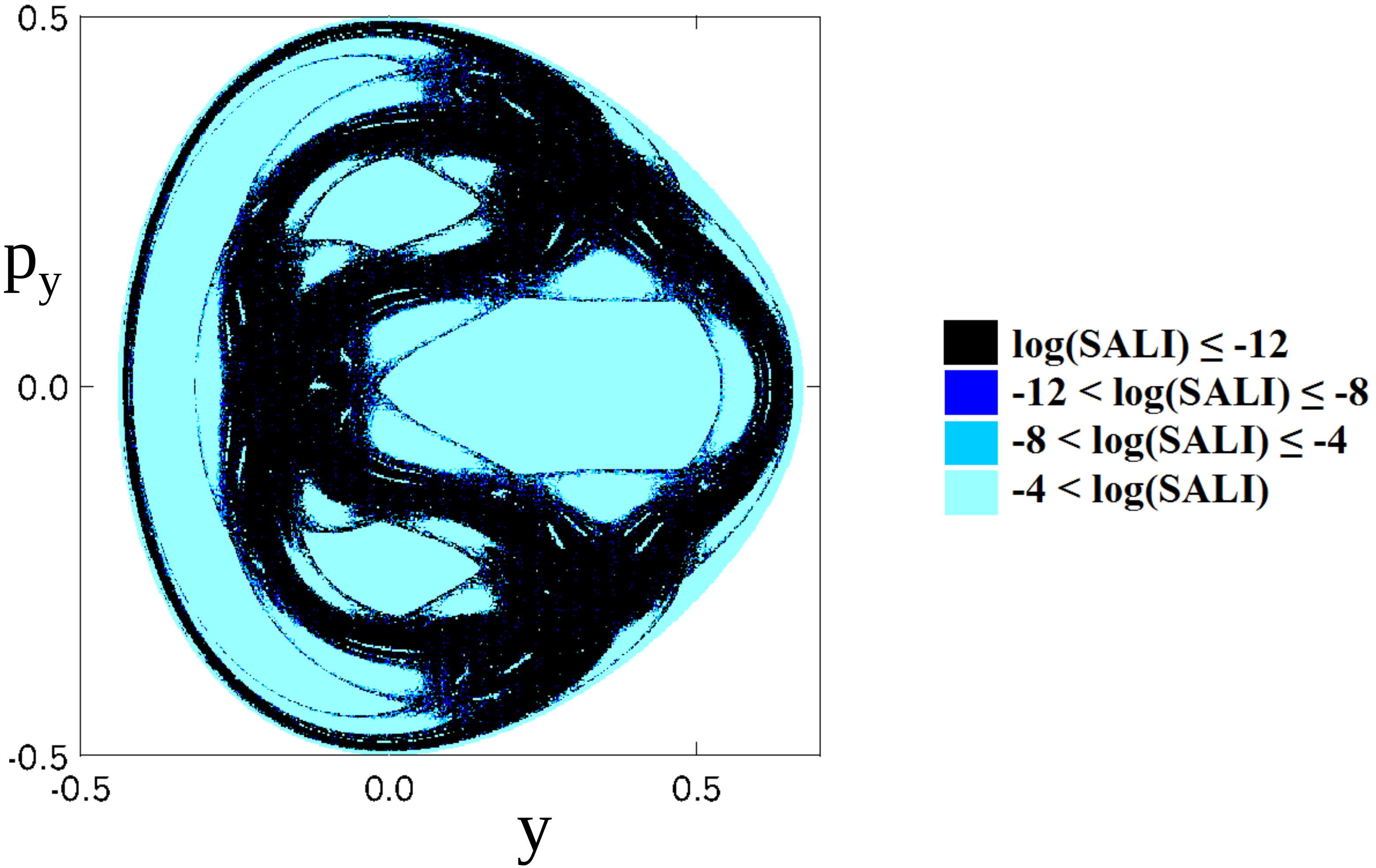

Applications – 4D map

$$\begin{aligned}
x_1' &= x_1 + x_2 \\
x_2' &= x_2 - \nu \sin(x_1 + x_2) - \mu[1 - \cos(x_1 + x_2 + x_3 + x_4)] \\
x_3' &= x_3 + x_4 \\
x_4' &= x_4 - \kappa \sin(x_3 + x_4) - \mu[1 - \cos(x_1 + x_2 + x_3 + x_4)]
\end{aligned} \quad (\text{mod } 2\pi)$$

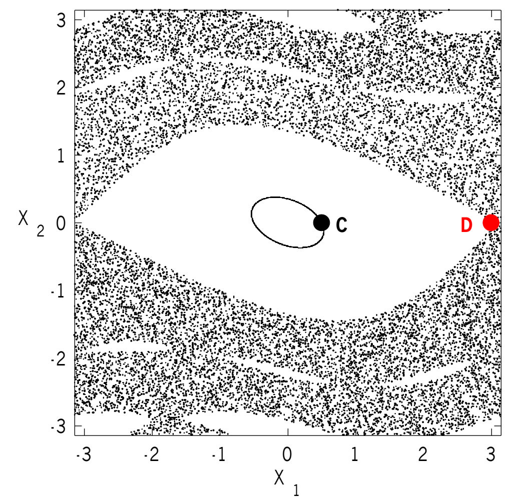

For ν=0.5, κ=0.1, μ=0.1 we consider the orbits:
regular orbit C *with initial conditions $x_1=0.5$, $x_2=0$, $x_3=0.5$, $x_4=0$.*
chaotic orbit D *with initial conditions $x_1=3$, $x_2=0$, $x_3=0.5$, $x_4=0$.*

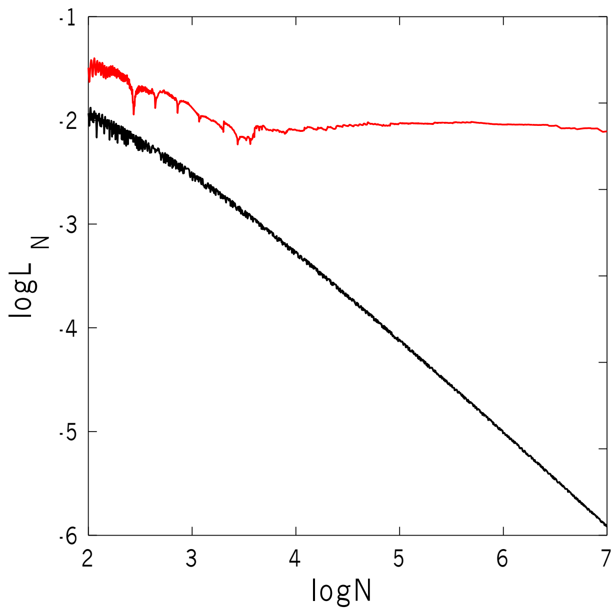

S., J. Phys. A (2001)

Applications – 4D map

$$\begin{aligned} x_1' &= x_1 + x_2 \\ x_2' &= x_2 - \nu \sin(x_1 + x_2) - \mu[1 - \cos(x_1 + x_2 + x_3 + x_4)] \\ x_3' &= x_3 + x_4 \\ x_4' &= x_4 - \kappa \sin(x_3 + x_4) - \mu[1 - \cos(x_1 + x_2 + x_3 + x_4)] \end{aligned} \quad (\mathrm{mod}\ 2\pi)$$

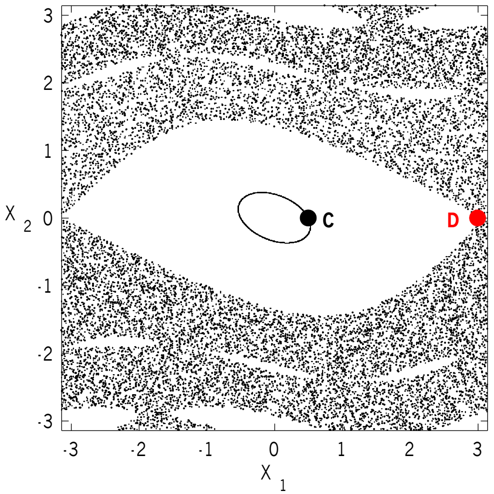

For ν=0.5, κ=0.1, μ=0.1 we consider the orbits:
regular orbit C *with initial conditions x_1=0.5, x_2=0, x_3=0.5, x_4=0.*
chaotic orbit D *with initial conditions x_1=3, x_2=0, x_3=0.5, x_4=0.*

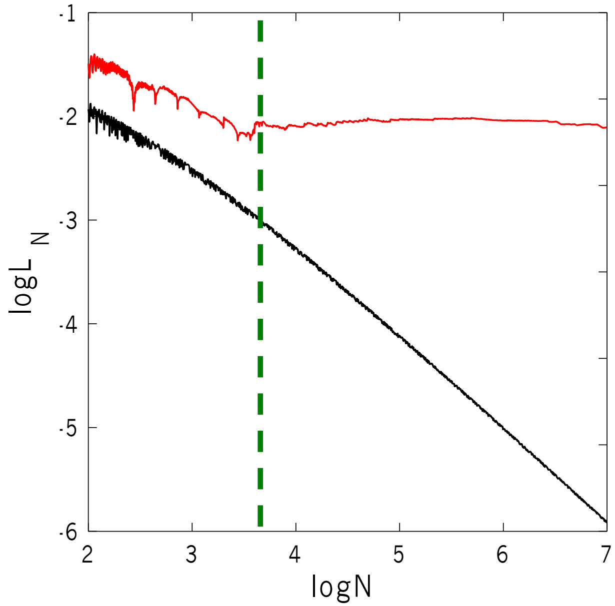

S., J. Phys. A (2001)

Applications – 4D map

$$
\begin{aligned}
x_1' &= x_1 + x_2 \\
x_2' &= x_2 - \nu \sin(x_1 + x_2) - \mu[1 - \cos(x_1 + x_2 + x_3 + x_4)] \\
x_3' &= x_3 + x_4 \\
x_4' &= x_4 - \kappa \sin(x_3 + x_4) - \mu[1 - \cos(x_1 + x_2 + x_3 + x_4)]
\end{aligned}
\quad (\text{mod } 2\pi)
$$

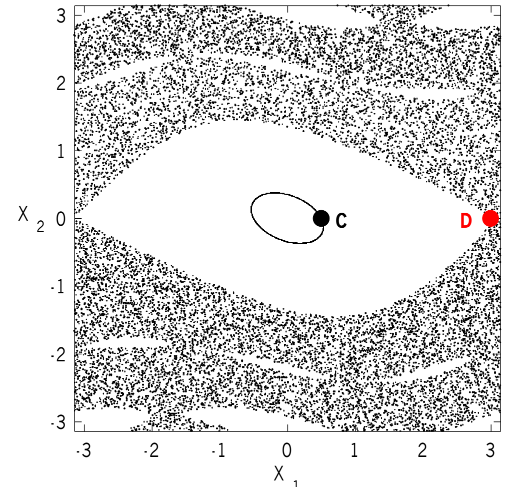

For ν=0.5, κ=0.1, μ=0.1 we consider the orbits:

regular orbit C *with initial conditions x_1=0.5, x_2=0, x_3=0.5, x_4=0.*

chaotic orbit D *with initial conditions x_1=3, x_2=0, x_3=0.5, x_4=0.*

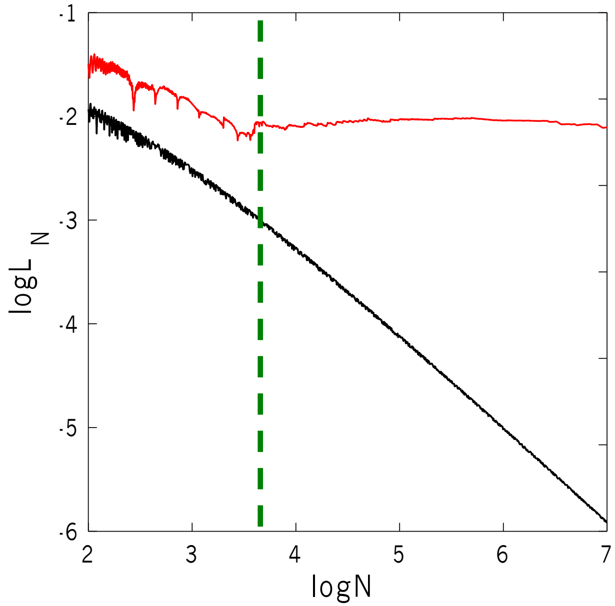

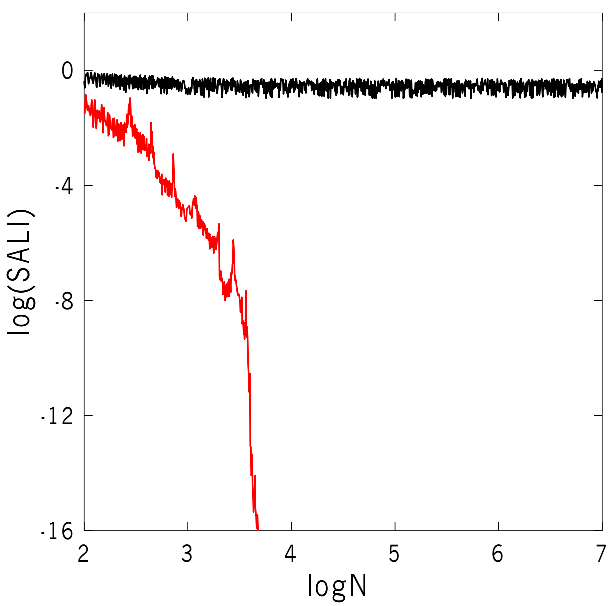

S., J. Phys. A (2001)

Applications – 4D map

$$
\begin{aligned}
x_1' &= x_1 + x_2 \\
x_2' &= x_2 - \nu \sin(x_1 + x_2) - \mu[1 - \cos(x_1 + x_2 + x_3 + x_4)] \\
x_3' &= x_3 + x_4 \\
x_4' &= x_4 - \kappa \sin(x_3 + x_4) - \mu[1 - \cos(x_1 + x_2 + x_3 + x_4)]
\end{aligned}
\quad (\mathrm{mod}\ 2\pi)
$$

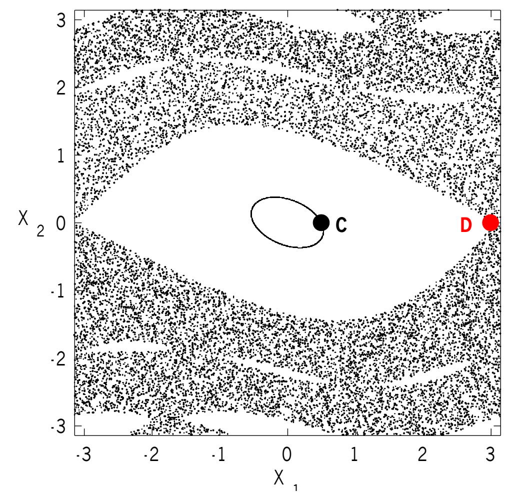

For ν=0.5, κ=0.1, μ=0.1 we consider the orbits:

regular orbit C *with initial conditions $x_1=0.5$, $x_2=0$, $x_3=0.5$, $x_4=0$.*

chaotic orbit D *with initial conditions $x_1=3$, $x_2=0$, $x_3=0.5$, $x_4=0$.*

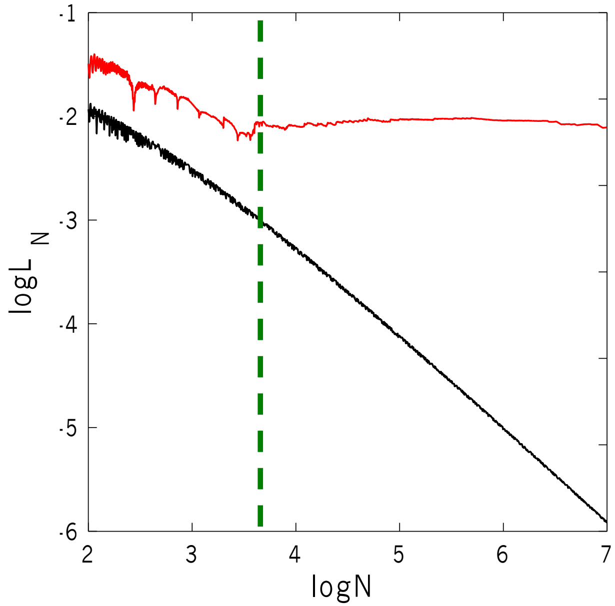

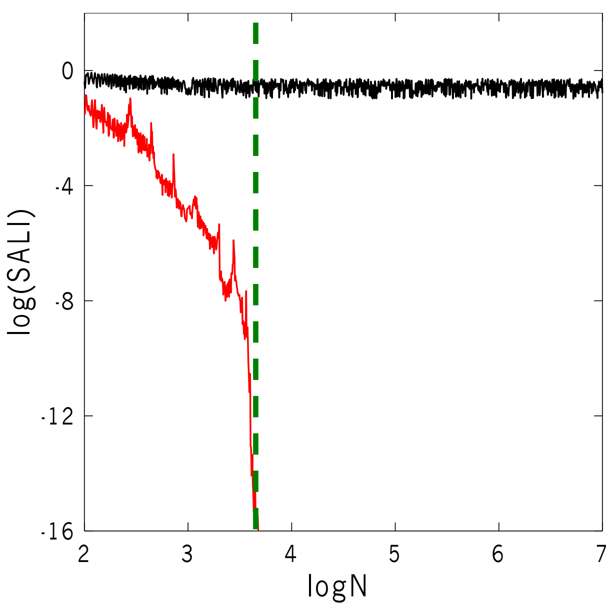

S., J. Phys. A (2001)

Applications – 2D map

$$\begin{aligned} x_1' &= x_1 + x_2 \\ x_2' &= x_2 - \nu \sin(x_1 + x_2) \end{aligned} \qquad (\mathrm{mod}\ 2\pi)$$

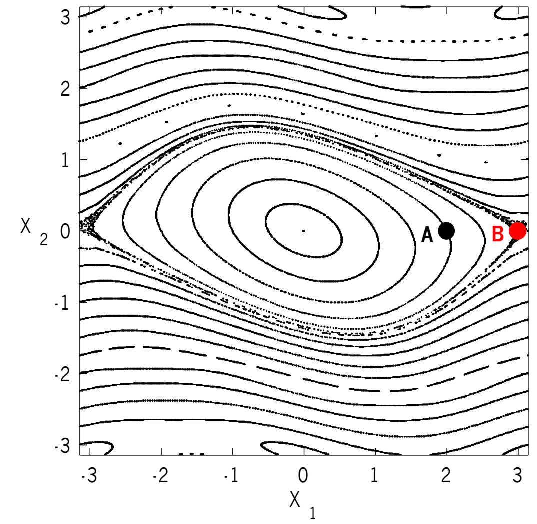

For ν=0.5 we consider the orbits:

***regular orbit* A** *with initial conditions x_1=2, x_2=0.*

***chaotic orbit B** with initial conditions x_1=3, x_2=0.*

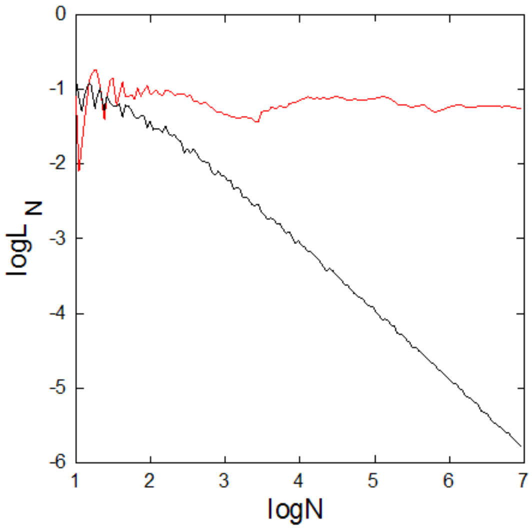

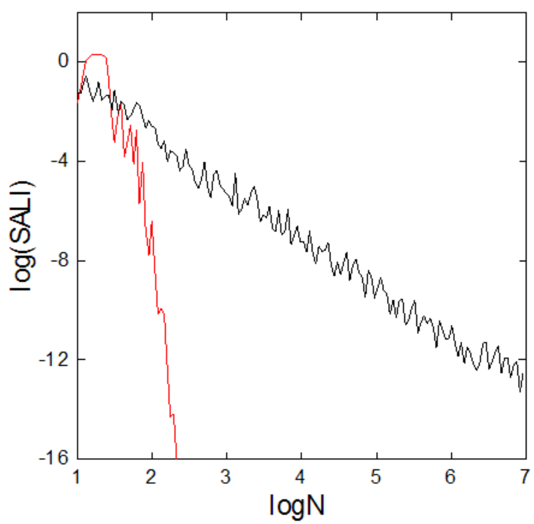

S., J. Phys. A (2001)

Behavior of the SALI

2D maps

SALI→0 both for regular and chaotic orbits

following, however, completely different time rates which allows us to distinguish between the two cases.

Hamiltonian flows and multidimensional maps

SALI→0 for chaotic orbits

SALI→constant ≠ 0 for regular orbits

The
Generalized ALignment Indices
(GALIs)
method

Definition of the Generalized Alignment Index (GALI)

SALI effectively measures the 'area' of the parallelogram formed by the two deviation vectors.

Definition of the Generalized Alignment Index (GALI)

SALI effectively measures the 'area' of the parallelogram formed by the two deviation vectors.

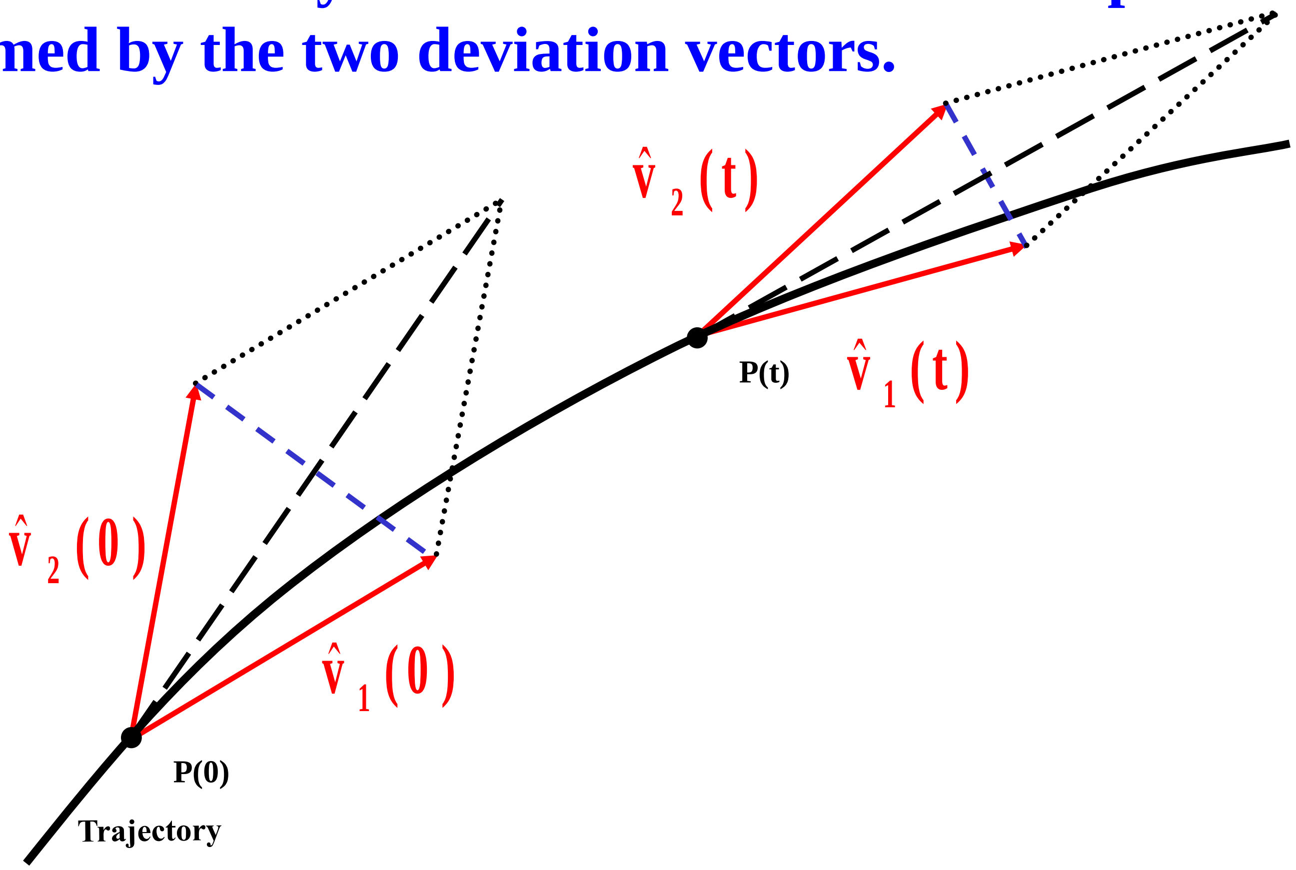

Definition of the Generalized Alignment Index (GALI)

SALI effectively measures the 'area' of the parallelogram formed by the two deviation vectors.

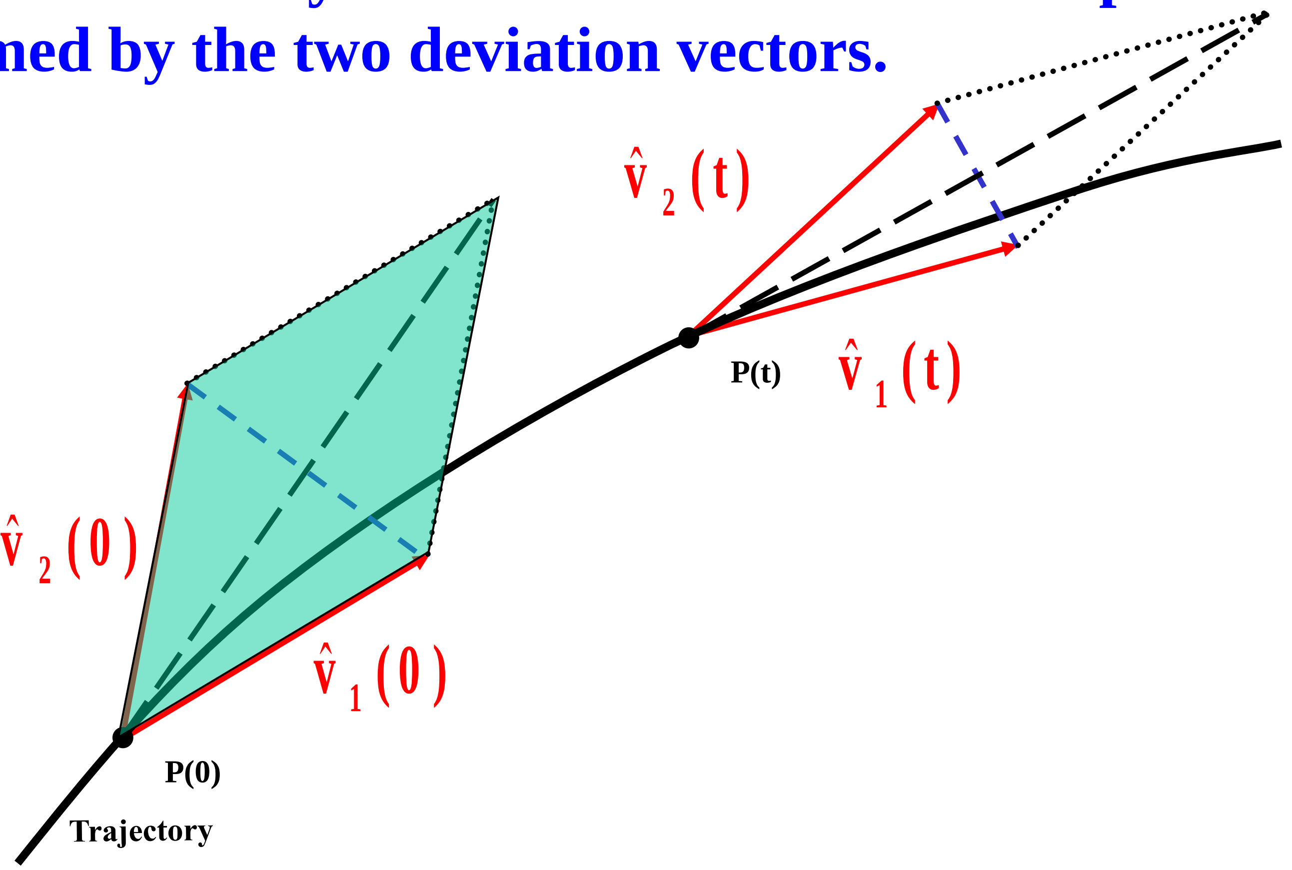

Definition of the Generalized Alignment Index (GALI)

SALI effectively measures the 'area' of the parallelogram formed by the two deviation vectors.

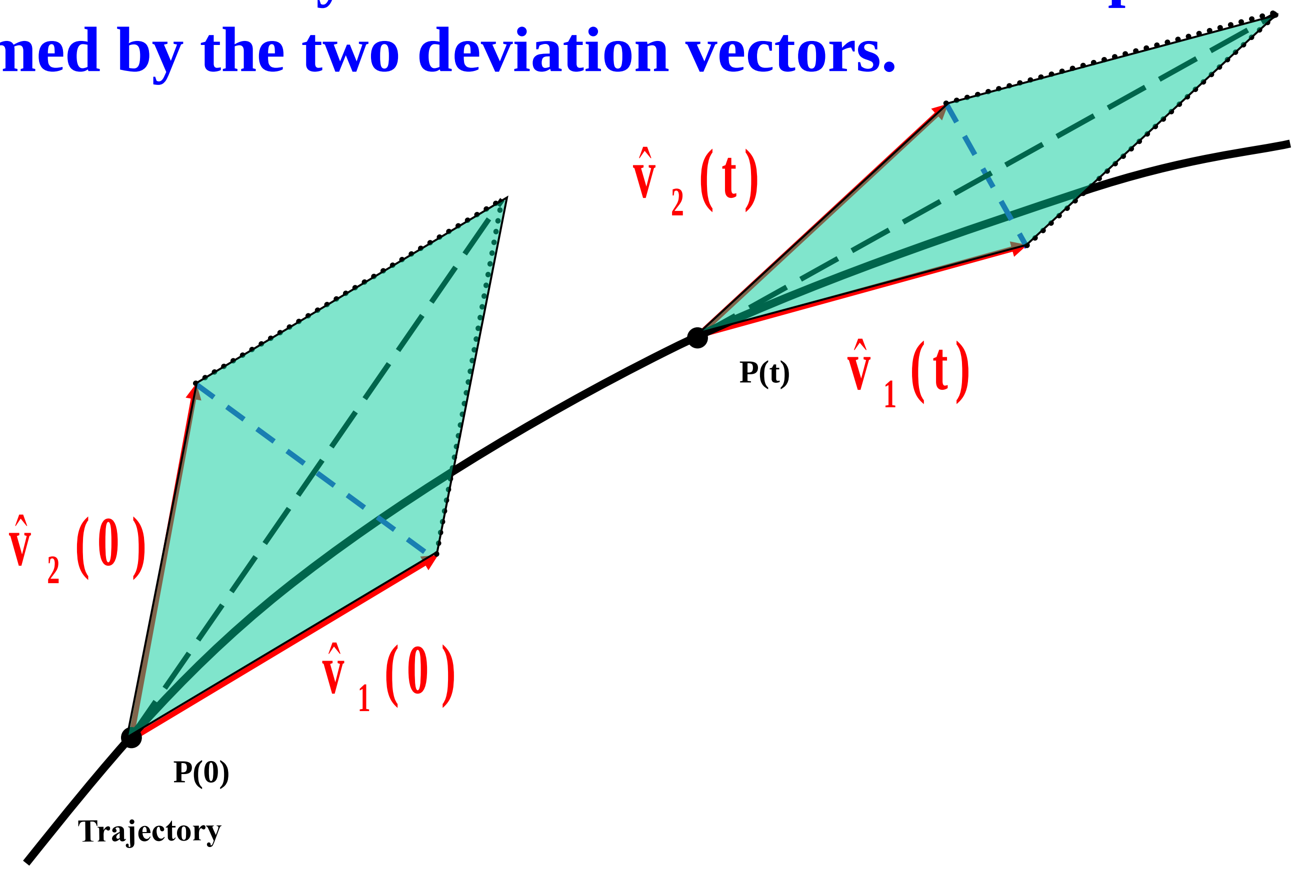

Definition of the Generalized Alignment Index (GALI)

SALI effectively measures the ‘area’ of the parallelogram formed by the two deviation vectors.

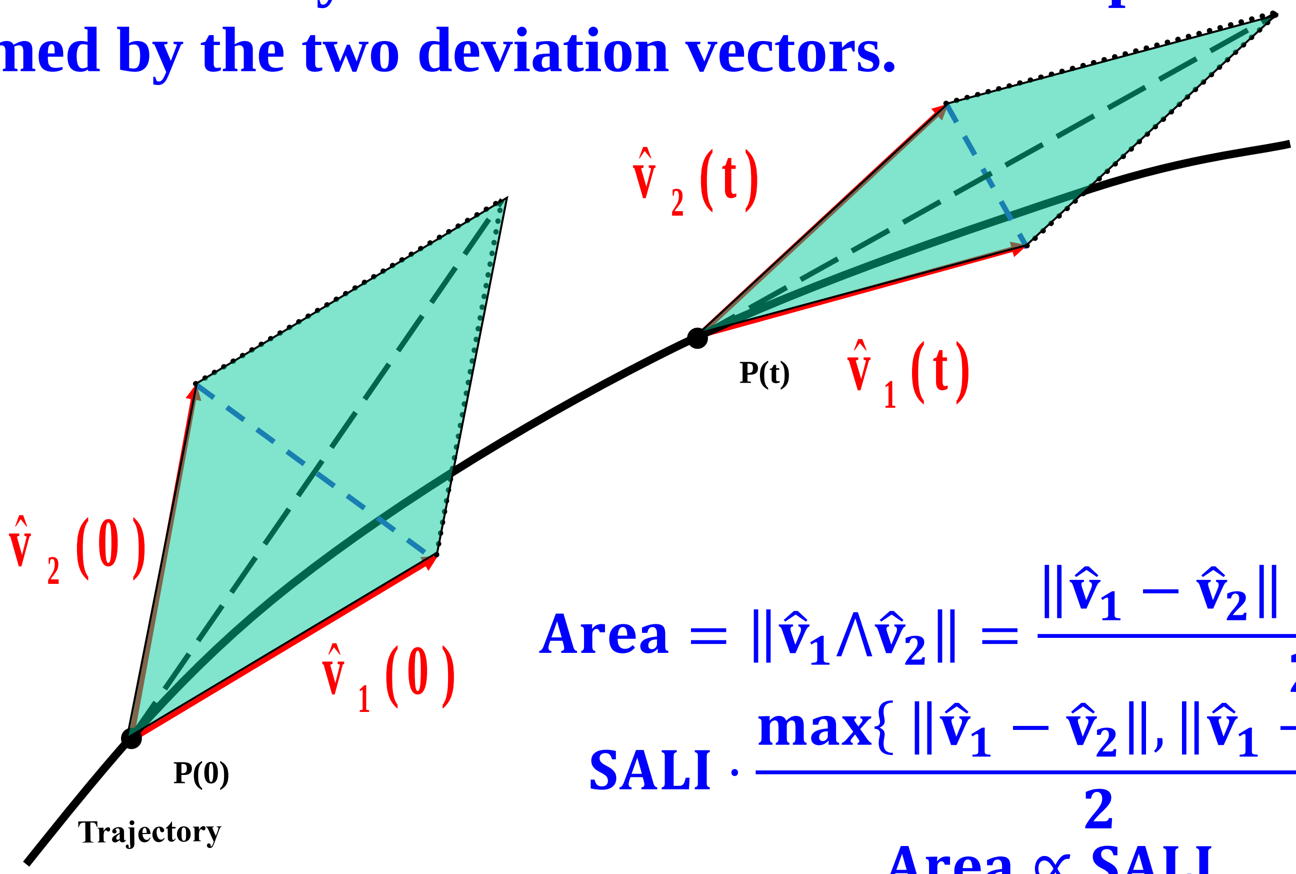

$$\mathbf{Area} = \|\hat{\mathbf{v}}_1 \wedge \hat{\mathbf{v}}_2\| = \frac{\|\hat{\mathbf{v}}_1 - \hat{\mathbf{v}}_2\| \cdot \|\hat{\mathbf{v}}_1 + \hat{\mathbf{v}}_2\|}{2} =$$

$$\mathbf{SALI} \cdot \frac{\max\{\|\hat{\mathbf{v}}_1 - \hat{\mathbf{v}}_2\|, \|\hat{\mathbf{v}}_1 + \hat{\mathbf{v}}_2\|\}}{2} \Rightarrow$$

$$\mathbf{Area} \propto \mathbf{SALI}$$

Definition of the Generalized Alignment Index (GALI)

In the case of an N degree of freedom Hamiltonian system we follow the evolution of k deviation vectors with $2 \leq k \leq 2N$, and define [S. et al., Physica D (2007)] the Generalized Alignment Index (GALI) of order k:

$$\boxed{\mathbf{GALI_k(t)} = \|\hat{\mathbf{v}}_1(\mathbf{t}) \wedge \hat{\mathbf{v}}_2(\mathbf{t}) \wedge \ldots \wedge \hat{\mathbf{v}}_k(\mathbf{t})\|}$$

where

$$\hat{\mathbf{v}}_1(\mathbf{t}) = \frac{\mathbf{v}_1(\mathbf{t})}{\|\mathbf{v}_1(\mathbf{t})\|}.$$

Note that $GALI_2$ (k=2) is equivalent to the Smaller Alignment Index (SALI).

Behavior of the $GALI_k$

Chaotic motion: $GALI_k$ ($2 \leq k \leq 2N$) tends exponentially to zero with exponents which involve the values of the first k largest Lyapunov exponents $\lambda_1, \lambda_2, \ldots, \lambda_k$:

$$\mathbf{GALI_k(t) \propto e^{-[(\lambda_1-\lambda_2)+(\lambda_1-\lambda_3)+\ldots+(\lambda_1-\lambda_k)]t}}$$

Regular motion: When the motion occurs on an N-dimensional torus then the behavior of $GALI_k$ is given by [S. et al., Physica D (2007) – S. et al., Eur. Phys. J. Sp. Top. (2008)]:

$$\mathbf{GALI_k(t) \propto \begin{cases} \text{constant} & \text{if} \quad 2 \leq k \leq N \\ \dfrac{1}{t^{2(k-N)}} & \text{if} \quad N < k \leq 2N \end{cases}}$$

Behavior of the $GALI_k$ for chaotic motion

N particles Fermi-Pasta-Ulam-Tsingou (FPUT) system:

$$H = \frac{1}{2}\sum_{i=1}^{N} p_i^2 + \sum_{i=0}^{N}\left[\frac{1}{2}(q_{i+1}-q_i)^2 + \frac{\beta}{4}(q_{i+1}-q_i)^4\right]$$

with fixed boundary conditions, N=8 and β=1.5.

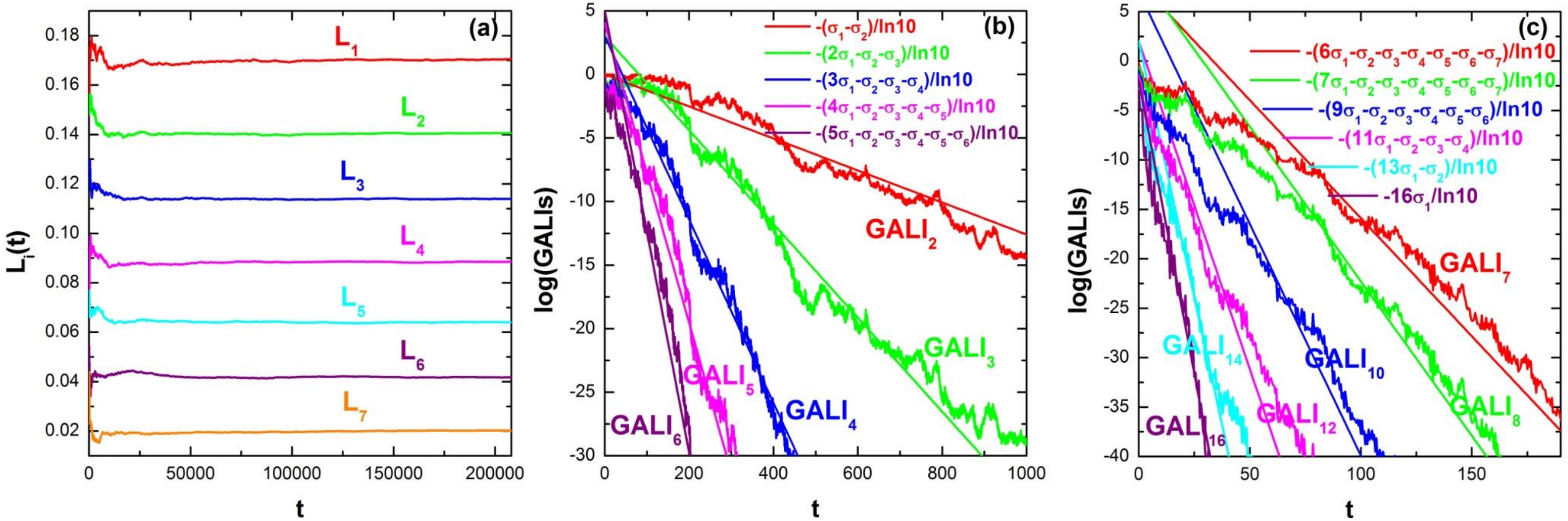

S. et al., Eur. Phys. J. Sp. Top. (2008)

Behavior of the $GALI_k$ for regular motion

N=8 FPUT system

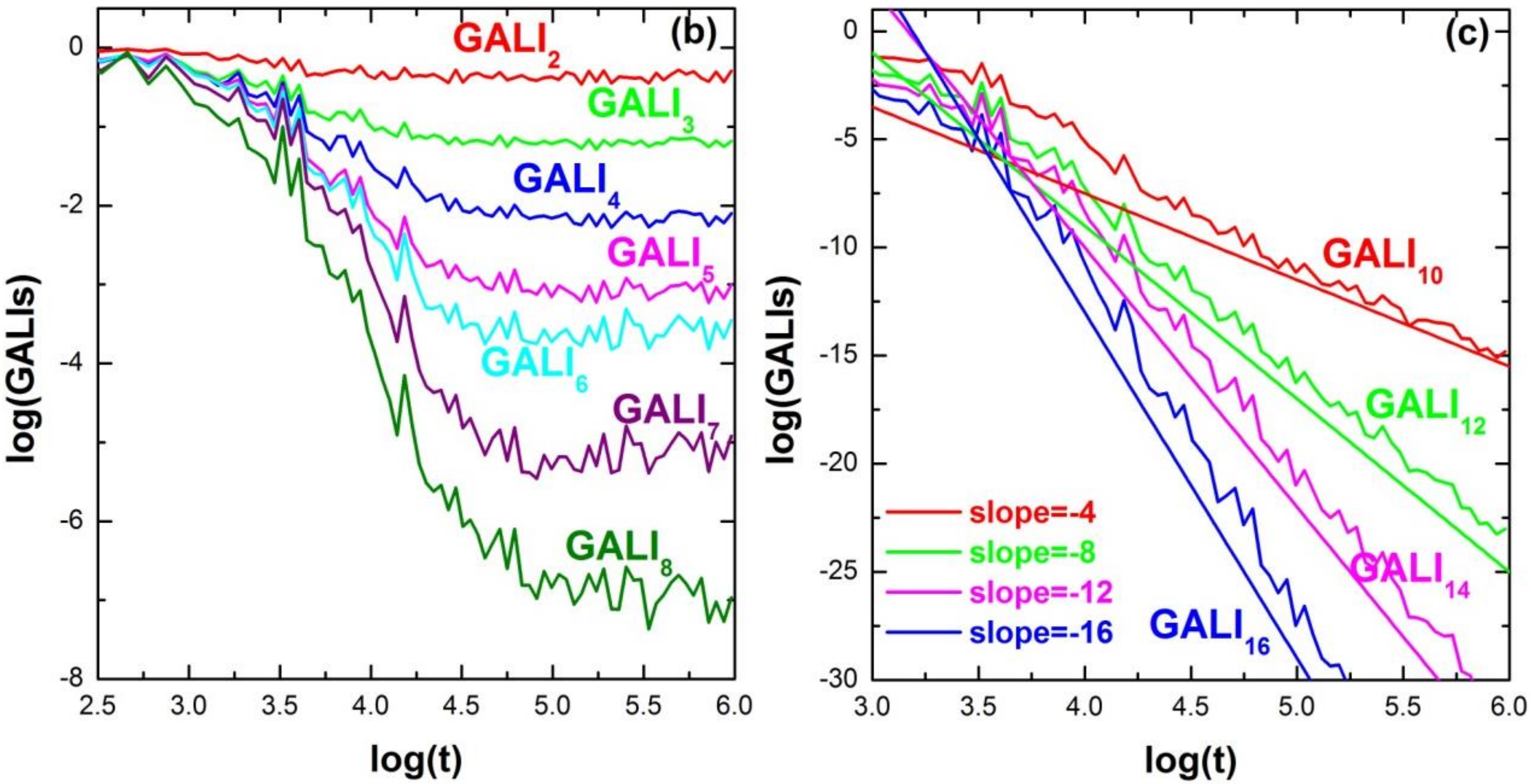

S. et al., Eur. Phys. J. Sp. Top. (2008)

Global dynamics

- **GALI$_2$ (practically equivalent to the use of SALI)**

- **GALI$_N$**

Chaotic motion: GALI$_N \rightarrow 0$ (exponential decay)

Regular motion:
GALI$_N \approx$ constant $\neq 0$

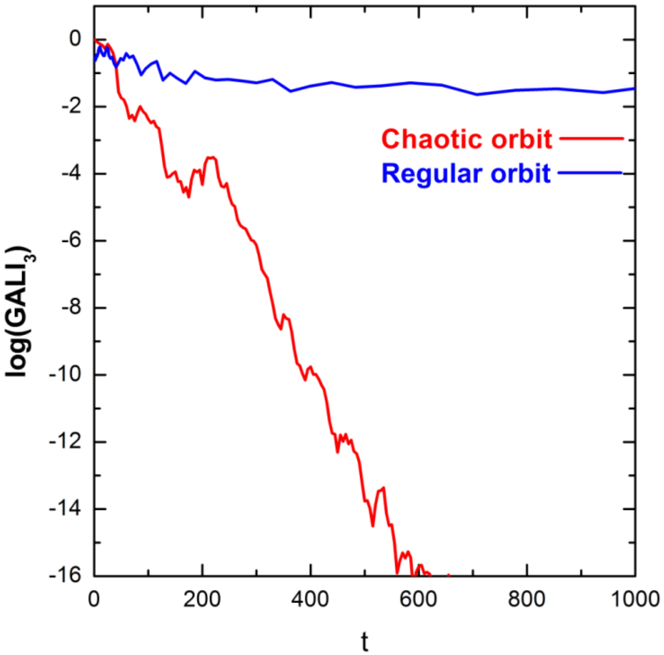

3D Hamiltonian
Subspace $q_3=p_3=0$, $p_2 \geq 0$ for $t=1000$.

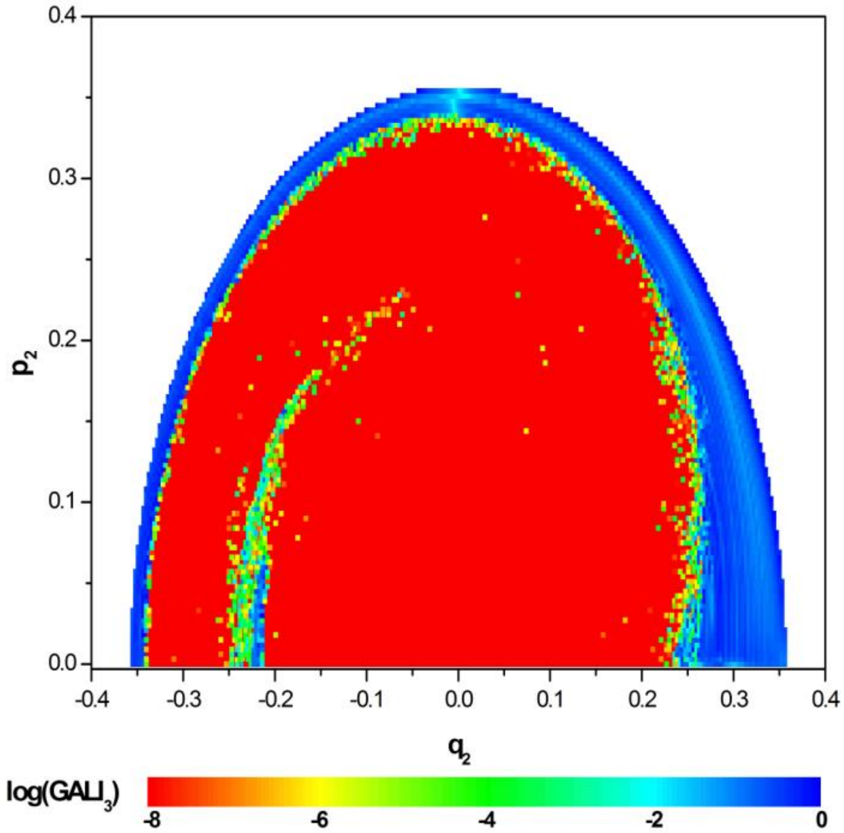

S. et al., Physica D (2007)

Global dynamics

GALI$_k$ with k>N

The index tends to zero both for regular and chaotic orbits but with completely different time rates:

Chaotic motion: exponential decay

Regular motion: power law

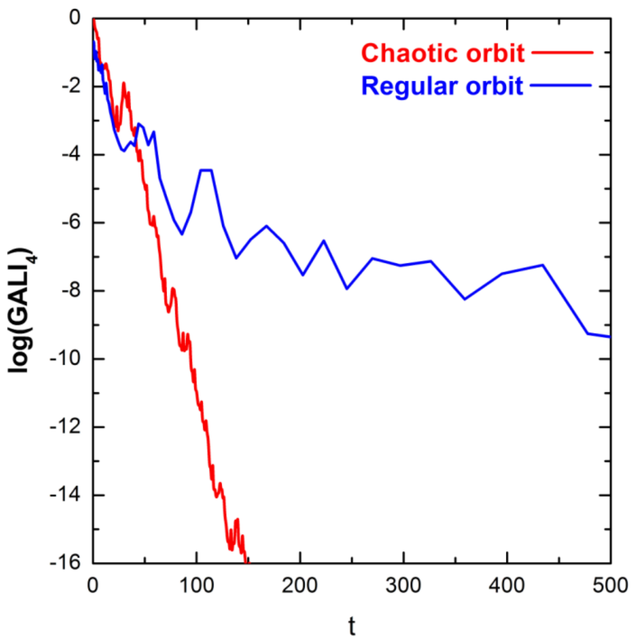

2D Hamiltonian (Hénon-Heiles)
Time needed for GALI$_4$<10^{-12}

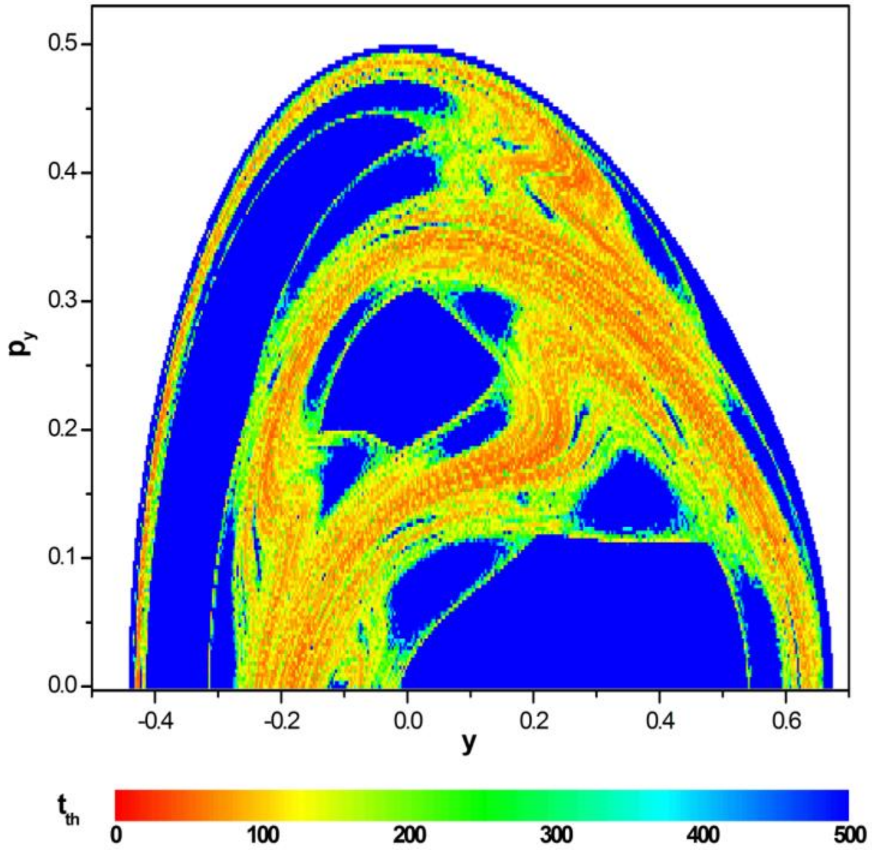

S. et al., Physica D (2007)

A time-dependent Hamiltonian system

Barred galaxies

NGC 1433

NGC 2217

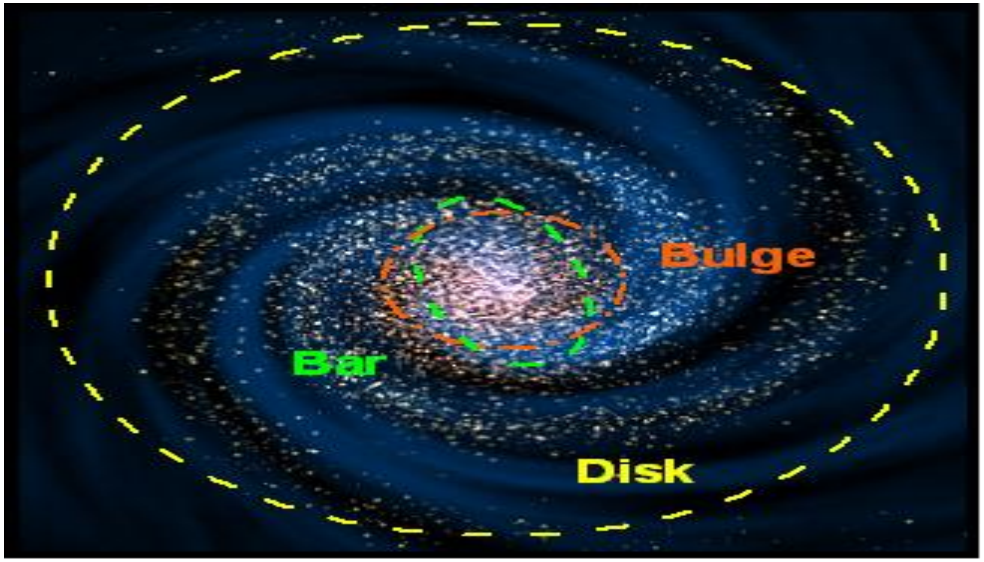

Barred galaxy model

The 3D bar rotates around its short *z*-axis (*x*: long axis and *y*: intermediate). The Hamiltonian that describes the motion for this model is:

$$H = \frac{1}{2}(p_x^2 + p_y^2 + p_z^2) + V(x,y,z) - \Omega_b (x p_y - y p_x) \equiv Energy$$

This model consists of the superposition of potentials describing an axisymmetric part and a bar component of the galaxy [Manos et al., J. Phys. A (2013)].

a) Axisymmetric component:

i) Plummer sphere:

$$V_{sphere}(x,y,z) = -\frac{GM_S}{\sqrt{x^2 + y^2 + z^2 + \varepsilon_s^{\ 2}}}$$

ii) Miyamoto–Nagai disc:

$$V_{disc}(x,y,z) = -\frac{GM_D}{\sqrt{x^2 + y^2 + (A + \sqrt{B^2 + z^2})^2}}$$

b) Bar component:

$$V_{bar}(x,y,z) = -\pi Gabc \frac{\rho_c}{n+1} \int_\lambda^\infty \frac{du}{\Delta(u)} (1 - m^2(u))^{n+1},$$

(Ferrers bar)

$$\boxed{\rho_c = \frac{105}{32\pi} \frac{GM_B}{abc}}$$

$$where\ m^2(u) = \frac{x^2}{a^2+u} + \frac{y^2}{b^2+u} + \frac{z^2}{c^2+u},\ \Delta^2(u) = (a^2+u)(b^2+u)(c^2+u),$$

n: positive integer ($n = 2$ for our model), λ: the unique positive solution of $m^2(\lambda) = 1$

Its density is:

$$\rho = \begin{cases} \rho_c (1 - m^2)^n, & \text{for } m \le 1 \\ 0, & \text{for } m > 1 \end{cases}, \text{ where } m^2 = \frac{x^2}{a^2} + \frac{y^2}{b^2} + \frac{z^2}{c^2},\ a > b > c \text{ and } n = 2.$$

Time-dependent barred galaxy model

The 3D bar rotates around its short *z*-axis (*x*: long axis and *y*: intermediate). The Hamiltonian that describes the motion for this model is:

$$H = \frac{1}{2}(p_x^2 + p_y^2 + p_z^2) + V(x,y,z,t) - \Omega_b(xp_y - yp_x) \equiv Energy$$

This model consists of the superposition of potentials describing an axisymmetric part and a bar component of the galaxy [Manos et al., J. Phys. A (2013)].

a) Axisymmetric component:

$$\boxed{M_S + M_B(t) + M_D(t) = 1, \quad \text{with} \quad M_B(t) = M_B(0) + \alpha t}$$

i) Plummer sphere:

$$V_{sphere}(x,y,z) = -\frac{GM_S}{\sqrt{x^2 + y^2 + z^2 + \varepsilon_s^2}}$$

ii) Miyamoto–Nagai disc:

$$V_{disc}(x,y,z) = -\frac{GM_D(t)}{\sqrt{x^2 + y^2 + (A + \sqrt{B^2 + z^2})^2}}$$

b) Bar component:

$$V_{bar}(x,y,z) = -\pi Gabc\frac{\rho_c}{n+1}\int_\lambda^\infty \frac{du}{\Delta(u)}(1 - m^2(u))^{n+1},$$

(Ferrers bar)

$$\boxed{\rho_c = \frac{105}{32\pi}\frac{GM_B(t)}{abc}}$$

$$\text{where } m^2(u) = \frac{x^2}{a^2+u} + \frac{y^2}{b^2+u} + \frac{z^2}{c^2+u}, \quad \Delta^2(u) = (a^2+u)(b^2+u)(c^2+u),$$

n: positive integer ($n = 2$ for our model), λ: the unique positive solution of $m^2(\lambda) = 1$

Its density is:

$$\rho = \begin{cases} \rho_c(1 - m^2)^n, & \text{for } m \le 1 \\ 0, & \text{for } m > 1 \end{cases}, \quad \text{where } m^2 = \frac{x^2}{a^2} + \frac{y^2}{b^2} + \frac{z^2}{c^2}, \quad a > b > c \text{ and } n = 2.$$

Time-dependent 2D barred galaxy model

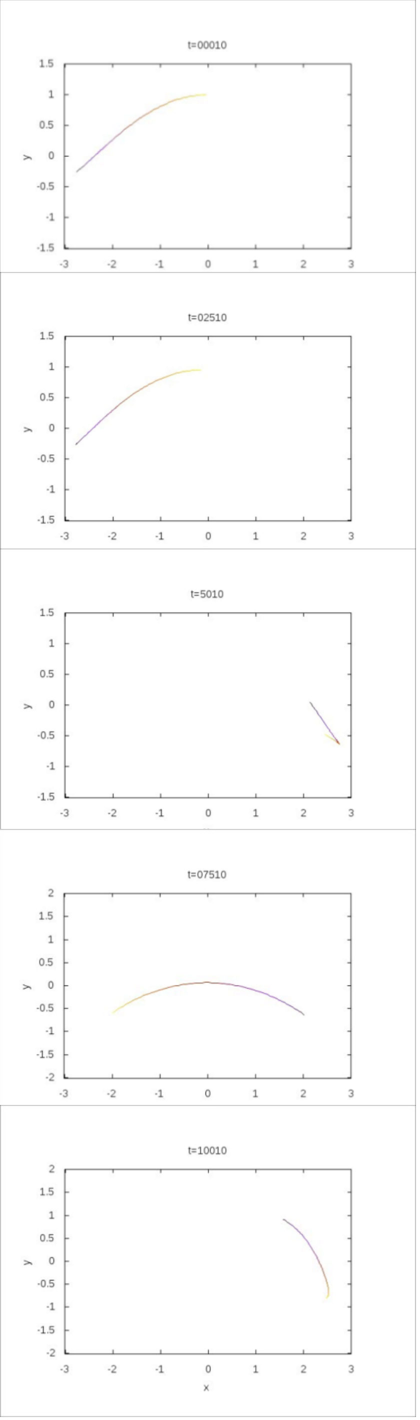

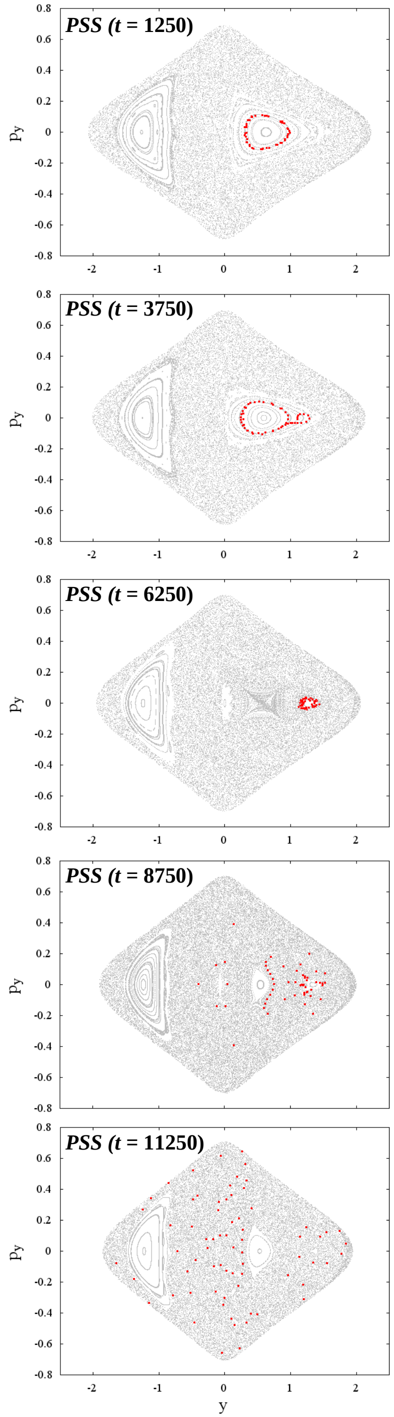

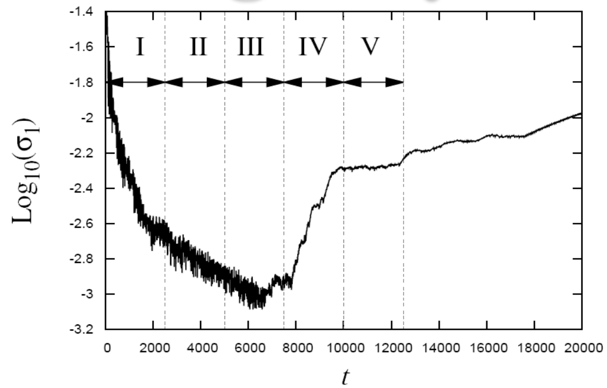

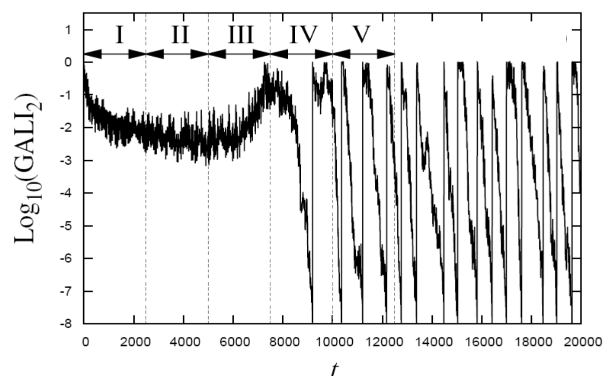

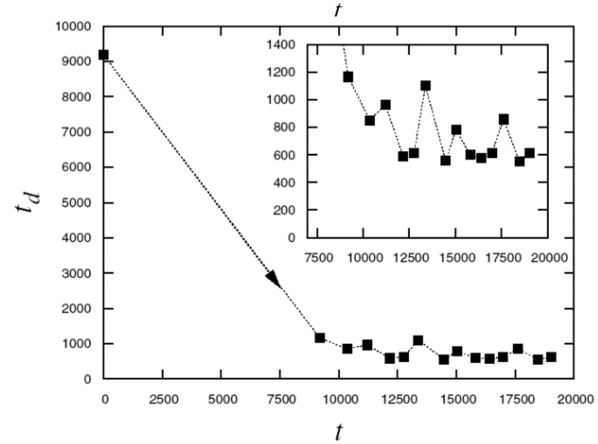

Time-dependent 3D barred galaxy model

Interplay between chaotic and regular motion

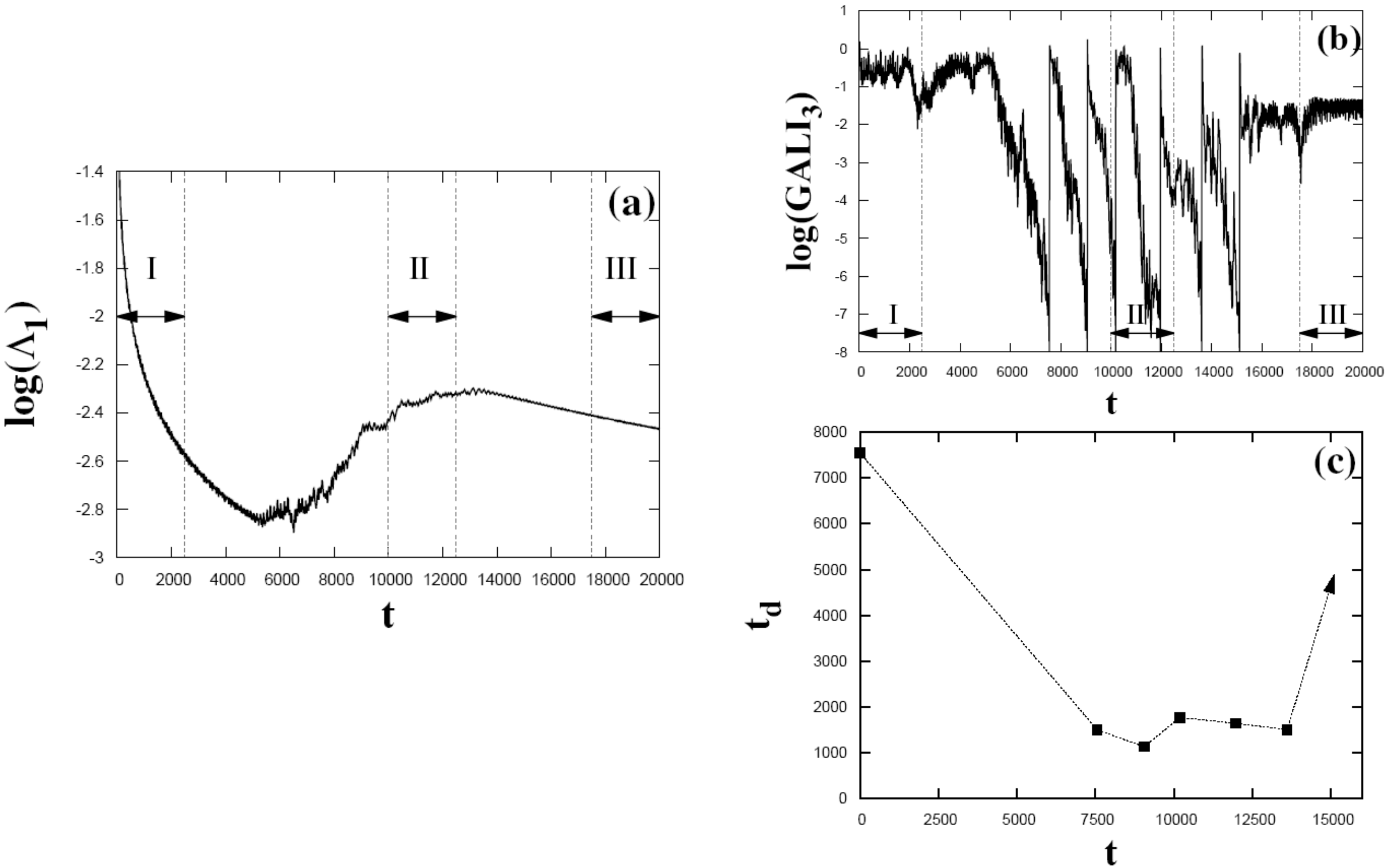

Chaos diagnostics based on Lagrangian descriptors (LDs)

Lagrangian descriptors (LDs)

The computation of LDs is based on the accumulation of some positive scalar value along the path of individual orbits.

Consider an *N* dimensional continuous time dynamical system

$$\dot{\mathbf{x}} = \frac{\mathbf{dx(t)}}{\mathbf{dt}} = \mathbf{f(x,t)}$$

The Arclength Definition [Madrid & Mancho, Chaos (2009) – Mendoza & Mancho, PRL (2010) – Mancho et al., Commun. Nonlin. Sci. Num. Simul. (2013)].

Forward time LD:

$$\mathbf{LD^f(x,\tau)} = \int_0^{\tau} \|\dot{\mathbf{x}}\mathbf{(t)}\|\mathbf{dt}$$

Backward time LD:

$$\mathbf{LD^b(x,\tau)} = \int_{-\tau}^{0} \|\dot{\mathbf{x}}\mathbf{(t)}\|\mathbf{dt}$$

Combined LD:

$$\mathbf{LD(x,\tau)} = \mathbf{LD^b(x,\tau)} + \mathbf{LD^f(x,\tau)}$$

LDs: 1 degree of freedom (dof) Hamiltonian

$$H(q,p) = \frac{1}{2}\left(p^2 - q^2\right)$$

The system has a hyperbolic fixed point at the origin. The LDs can be used to display the stable and unstable manifolds of this point.

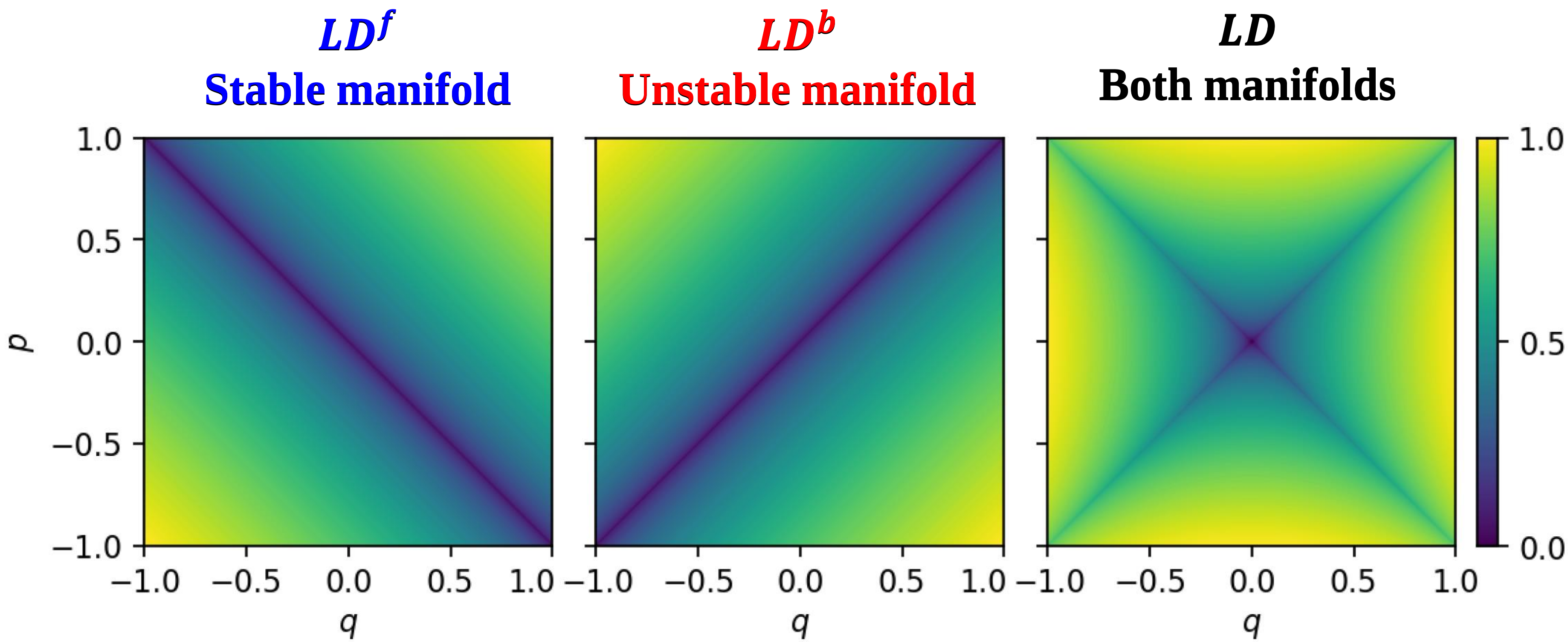

From Agaoglou et al. 'Lagrangian descriptors: Discovery and quantification of phase space structure and transport', 2020, https://doi.org/10.5281/zenodo.3958985

LDs: 1 dof Duffing Oscillator

$$H(x, y) = \frac{1}{2}y^2 + \frac{1}{4}x^4 - \frac{1}{2}x^2$$

The system has three equilibrium points: a saddle located at the origin and two diametrically opposed centers at the points (± 1, 0).

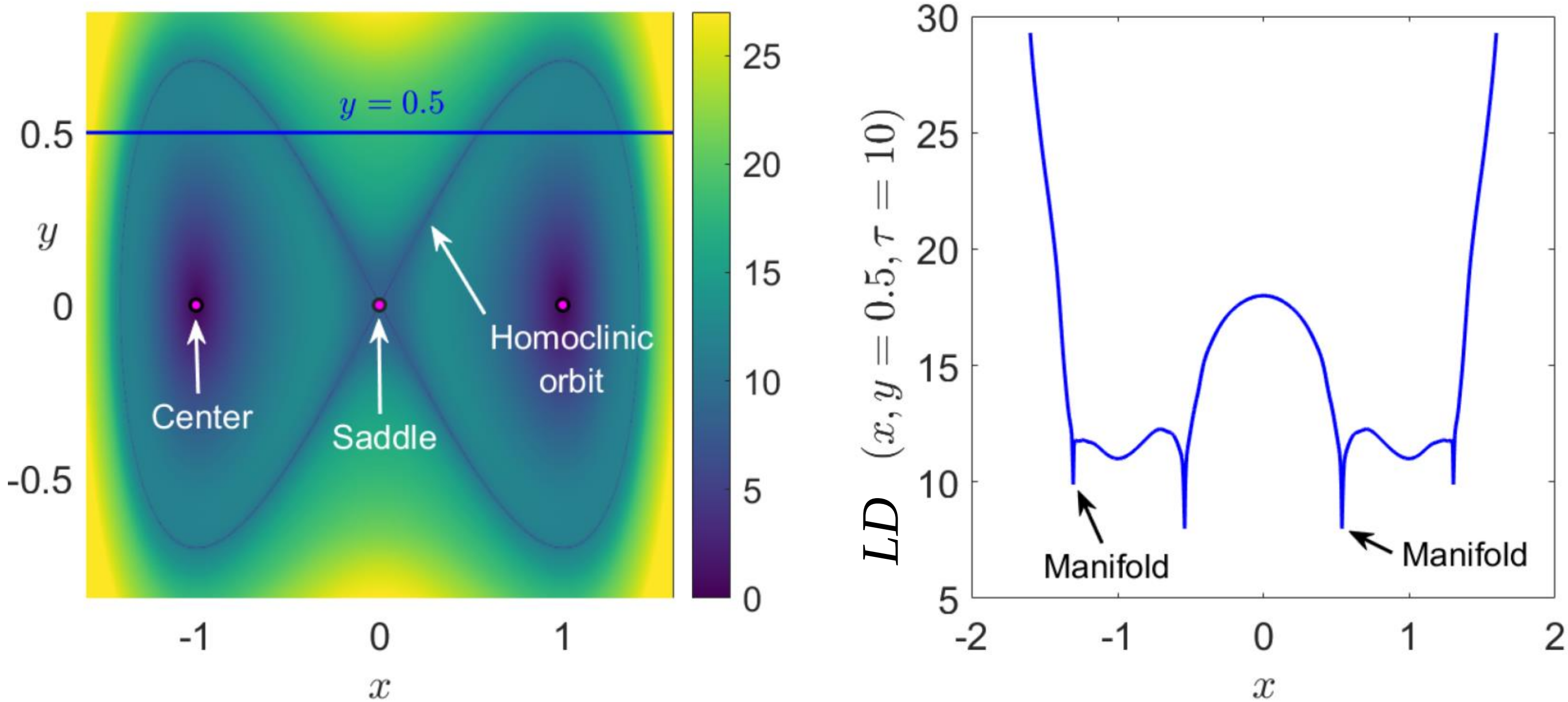

From Agaoglou et al. 'Lagrangian descriptors: Discovery and quantification of phase space structure and transport', 2020, https://doi.org/10.5281/zenodo.3958985

The location of the stable and unstable manifolds can be extracted from the ridges of the gradient field of the LDs since they are located at points where the forward and the backward components of the LD are non-differentiable.

Lagrangian descriptors (LDs)

The ‘p-norm’ Definition [Lopesino et al., Commun. Nonlin. Sci. Num. Simul. (2015) – Lopesino et al., Int. J. Bifurc. Chaos (2017)].

Combined *LD* (usually p=1/2):

$$\mathbf{LD}(\mathbf{x},\boldsymbol{\tau}) = \int_{-\tau}^{\tau}\left(\sum_{i=1}^{N}|\mathbf{f_i}(\mathbf{x},\mathbf{t})|^{\mathbf{p}}\right)\mathbf{dt}$$

Hénon-Heiles system: $\mathbf{H} = \frac{1}{2}\left(\mathbf{p_x^2}+\mathbf{p_y^2}\right)+\frac{1}{2}\left(\mathbf{x^2}+\mathbf{y^2}\right)+\mathbf{x^2y}-\frac{1}{3}\mathbf{y^3}$

Stable and unstable manifolds for H=1/3, τ=10.

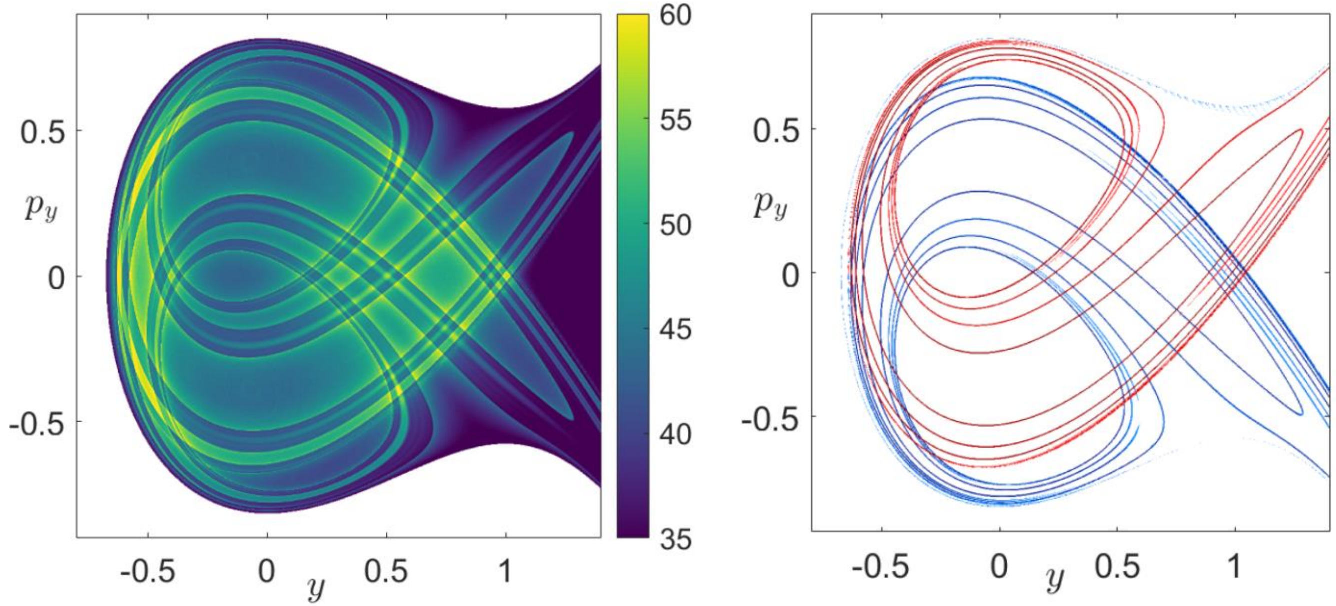

From Agaoglou et al. ‘Lagrangian descriptors: Discovery and quantification of phase space structure and transport’, 2020, https://doi.org/10.5281/zenodo.3958985

Using LDs to quantify chaos

We consider orbits on a finite grid of an n(≥1)-dimensional subspace of the N(≥n)-dimensional phase space of a dynamical system and their LDs.
Any non-boundary point x in this subspace has 2n nearest neighbors

$$\mathbf{y_i^{\pm} = x \pm \sigma^{(i)} e^{(i)}, \qquad i = 1, 2, \dots, n,}$$

where $\mathbf{e^{(i)}}$ is the ith usual basis vector in $\mathbb{R}^n$ and $\boldsymbol{\sigma}^{(i)}$ is the distance between successive grid points in this direction.

The difference $\mathbf{D_L^n}$ of neighboring orbits' LDs:

$$\mathbf{D_L^n(x) = \frac{1}{2n} \sum_{i=1}^{n} \frac{\left|LD^f(x) - LD^f(y_i^+)\right| + \left|LD^f(x) - LD^f(y_i^-)\right|}{LD^f(x)}}.$$

The ratio $\mathbf{R_L^n}$ of neighboring orbits' LDs:

$$\mathbf{R_L^n(x) = \left| 1 - \frac{1}{2n} \sum_{i=1}^{n} \frac{LD^f(y_i^+) + LD^f(y_i^-)}{LD^f(x)} \right|}.$$

Hillebrand et al., Chaos (2022) – Zimper et al., Physica D (2023)

Application: Hénon-Heiles system

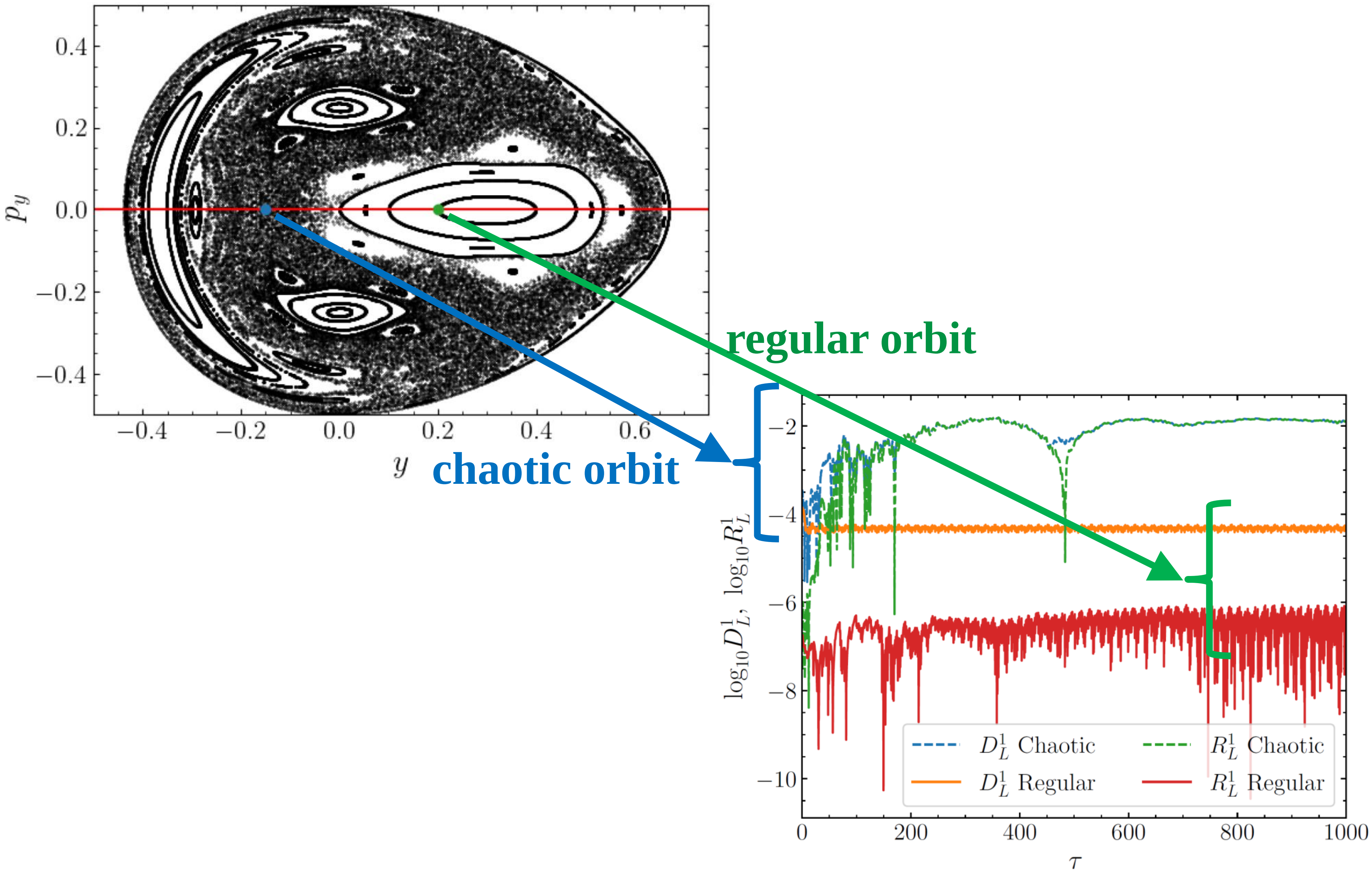

Application: Hénon-Heiles system

H=1/8

LDs for $\tau=10^3$

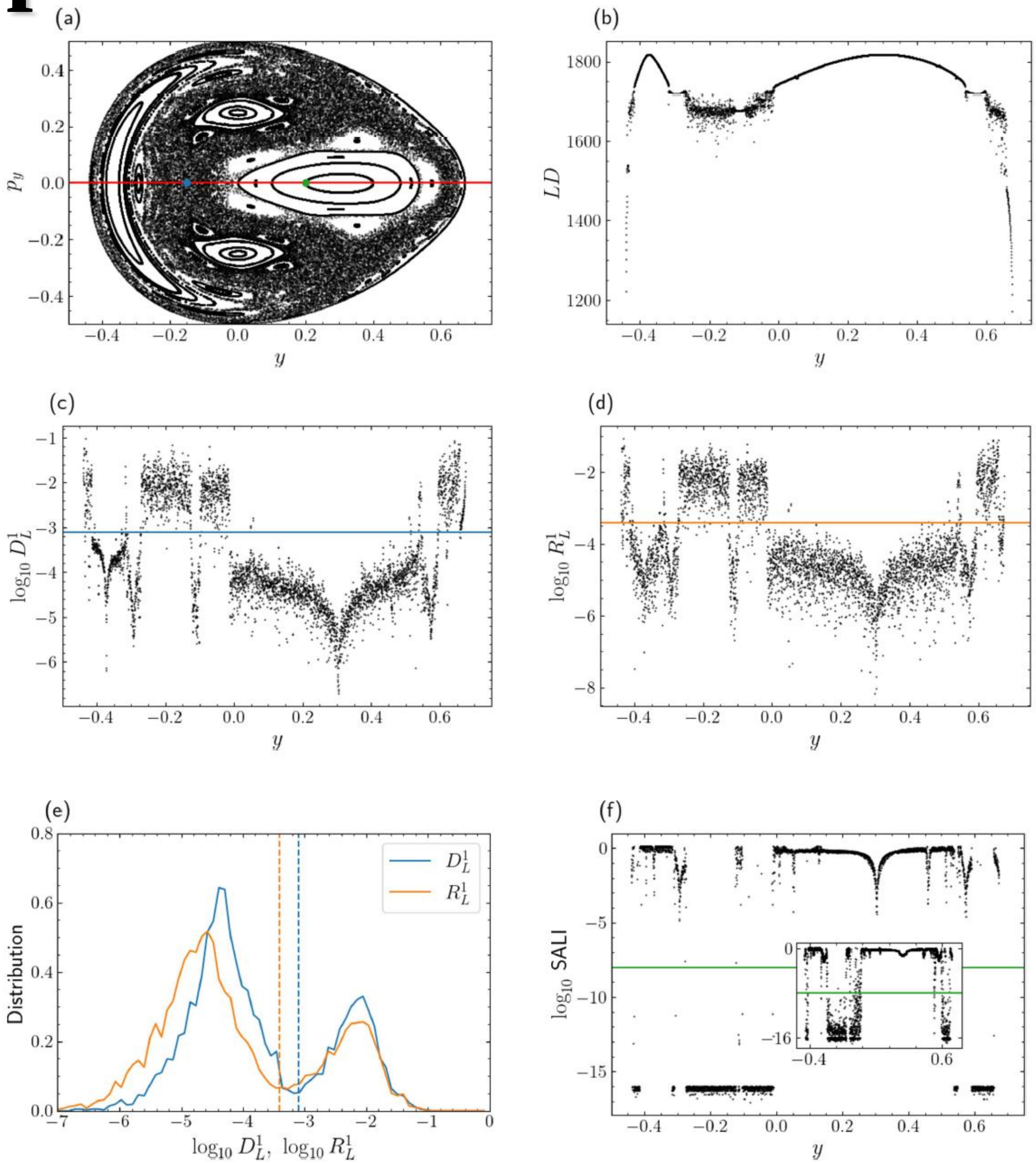

Variation of LDs with regard to initial conditions.

regular regions: smooth

chaotic regions: erratic

[also see Montes et al., Commun. Nonlin. Sci. Num. Simul. (2021)]

SALI for $\tau=10^6$ (inset $\tau=10^3$)

Application: Hénon-Heiles system

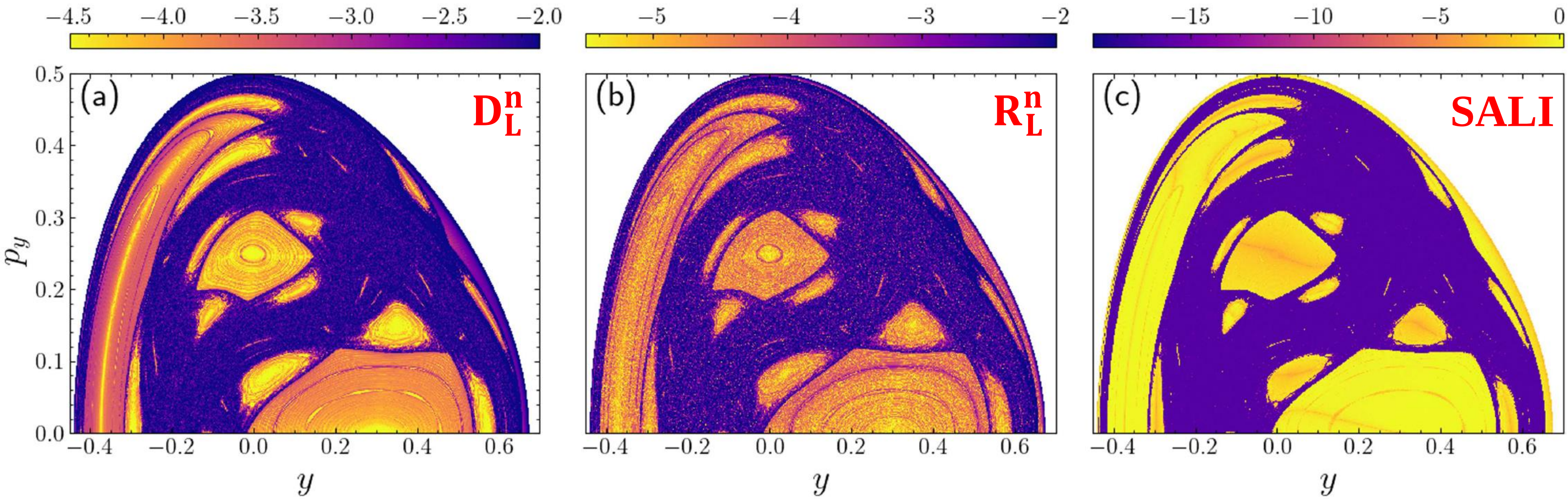

Misclassified orbits (< 10%)

D_L^n

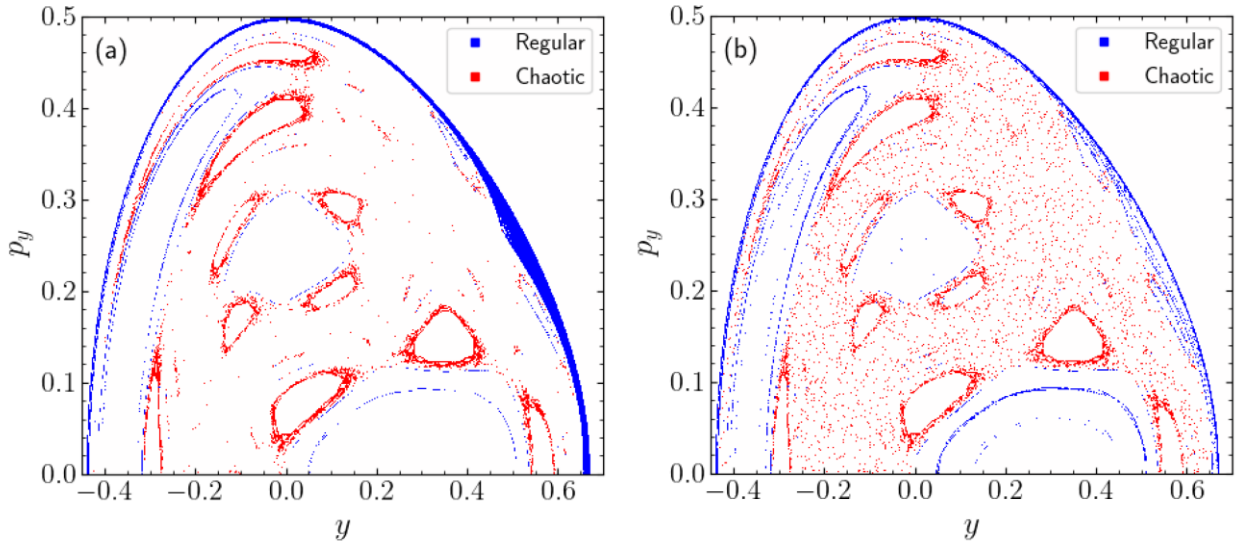

R_L^n

Application: Hénon-Heiles system

A quantity related to the second derivative of the LDs was introduced in Daquin et al., Physica D (2022) and was used in Hillebrand et al., Chaos (2022) and Zimper et al., Physica D (2023):

$$\|\Delta \mathrm{LD}\|(\mathbf{x}) = \left|\frac{\mathrm{LD}^{f}(\mathbf{y}_i^{+}) - 2\mathrm{LD}^{f}(\mathbf{x}) + \mathrm{LD}^{f}(\mathbf{y}_i^{-})}{\sigma^2}\right|.$$

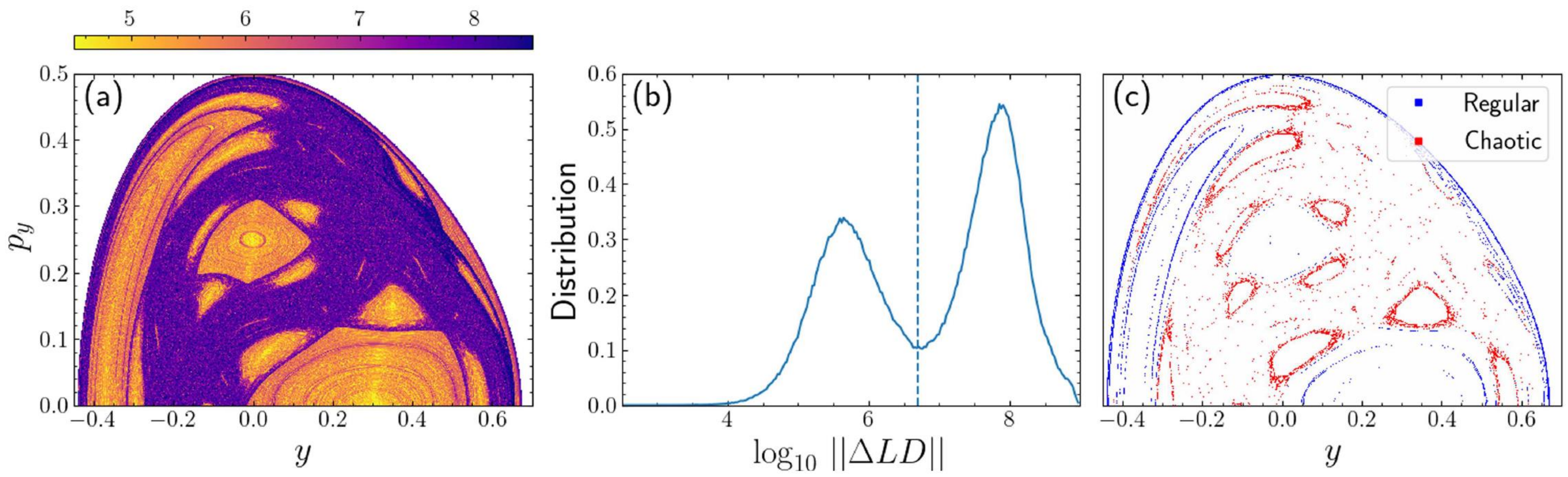

Summary I

- We discussed methods of chaos detection based on
  - ✓ the visualization of orbits
  - ✓ the numerical analysis of orbits
  - ✓ the evolution of deviation vectors (variational equations – tangent map)
- The Smaller (SALI) and the Generalized (GALI) ALignment Index methods are fast, efficient and easy to compute chaos indicator.
- Behaviour of the Generalized ALignment Index of order k ($GALI_k$):
  - ✓ Chaotic motion: it tends exponentially to zero
  - ✓ Regular motion: it fluctuates around non-zero values (or goes to zero following power-laws)
- $GALI_k$ indices :
  - ✓ can distinguish rapidly and with certainty between regular and chaotic motion
  - ✓ can be used to characterize individual orbits as well as "chart" chaotic and regular domains in phase space
  - ✓ can identify regular motion on low–dimensional tori
  - ✓ are perfectly suited for studying the global dynamics of multidimentonal systems, as well as of time-dependent models

Summary II

- **We introduced and successfully implemented computationally efficient ways to effectively identify chaos in conservative dynamical systems from the values of LDs at neighboring initial conditions.**
- **From the distributions of the indices' values we determine appropriate threshold values, which allow the characterization of orbits as regular or chaotic.**
- **Both indices faced problems in correctly revealing the nature of some orbits mainly at the borders of stability islands.**
- **Both indices show overall very good performance, as their classifications are in accordance with the ones obtained by the SALI at a level of at least 90% agreement.**
- **Advantages:**
  - ✓ **Easy to compute (actually only the forward LDs are needed).**
  - ✓ **No need to know and to integrate the variational equations.**
- **These methods has also been successfully applied to 2D and 4D symplectic maps [Hillebrand et al., Chaos (2022) – Zimper et al., Physica D (2023)]**

Main References I

- The color and rotation (CR) method
  - ✓ Patsis & Zachilas (1994) Int. J. Bif. Chaos, 4, 1399
  - ✓ Katsanikas & Patsis (2011) Int. J. Bif. Chaos, 21, 467
  - ✓ Katsanikas, Patsis & Contopoulos (2011) Int. J. Bif. Chaos, 21, 2321

- the 3D phase space slices (3PSS) technique
  - ✓ Richter, Lange, Backer & Ketzmerick (2014), Phys. Rev. E 89, 022902
  - ✓ Lange, Richter, Onken, Backer & Ketzmerick (2014), Chaos 24, 024409
  - ✓ Onken, Lange, Ketzmerick & Backer (2016), Chaos 26, 063124

- Frequency Analysis
  - ✓ Laskar (1990) Icarus, 88, 266
  - ✓ Laskar, Froeschle &Celletti (1992) Physica D, 56, 253
  - ✓ Laskar (1993) Physica D, 67, 257
  - ✓ Bartolini, Bazzani, Giovannozzi, Scandale & Todesco (1996) Part. Accel. 52, 147
  - ✓ Laskar (1999) in Hamiltonian systems with three or more degrees of freedom (ed. Simo / Plenum Press) p 134

- Lyapunov exponents
  - ✓ Oseledec (1968) Trans. Moscow Math. Soc., 19, 197
  - ✓ Benettin, Galgani, Giorgilli & Strelcyn (1980) Meccanica, March, 9
  - ✓ Benettin, Galgani, Giorgilli & Strelcyn (1980) Meccanica, March, 21
  - ✓ Wolf, Swift, Swinney & Vastano (1985) Physica D, 16, 285
  - ✓ S. (2010) Lect. Notes Phys., 790, 63

Main References II

- **0-1 test**
  - ✓ **Gottwald & Melbourne (2004) Proc. R. Soc. A, 460, 603**
  - ✓ **Gottwald & Melbourne (2005) Physica D, 212, 100**
  - ✓ **Gottwald & Melbourne (2009) SIAM J. Appl. Dyn., 8, 129**
  - ✓ **Gottwald & Melbourne (2016) Lect. Notes Phys., 915, 221**

- **FLI – OFLI – OFLI2**
  - ✓ **Froeschle, Lega & Gonczi (1997) Celest. Mech. Dyn. Astron., 67, 41**
  - ✓ **Guzzo, Lega & Froeschle (2002) Physica D, 163, 1**
  - ✓ **Fouchard, Lega, Froeschle & Froeschle (2002) Celest. Mech. Dyn. Astron., 83, 205**
  - ✓ **Barrio (2005) Chaos Sol. Fract., 25, 71**
  - ✓ **Barrio (2006) Int. J. Bif. Chaos, 16, 2777**
  - ✓ **Lega, Guzzo & Froeschle (2016) Lect. Notes Phys., 915, 35**
  - ✓ **Barrio (2016) Lect. Notes Phys., 915, 55**

- **MEGNO**
  - ✓ **Cincotta & Simo (2000) Astron. Astroph. Suppl. Ser., 147, 205**
  - ✓ **Cincotta, Giordano & Simo (2003) Physica D, 182, 151**
  - ✓ **Cincotta, & Giordano (2016) Lect. Notes Phys., 915, 93**

- **RLI**
  - ✓ **Sandor, Erdi & Efthymiopoulos (2000) Celest. Mech. Dyn. Astron., 78, 113**
  - ✓ **Sandor, Erdi, Szell & Funk (2004) Celest. Mech. Dyn. Astron., 90 127**
  - ✓ **Sandor & Maffione (2016) Lect. Notes Phys., 915, 183**

Main References III

- **SALI**
  - ✓ S. (2001) J. Phys. A, 34, 10029
  - ✓ S., Antonopoulos, Bountis & Vrahatis (2003) Prog. Theor. Phys. Supp., 150, 439
  - ✓ S., Antonopoulos, Bountis & Vrahatis (2004) J. Phys. A, 37, 6269
  - ✓ Bountis & S. (2006) Nucl. Inst Meth. Phys Res. A, 561, 173
  - ✓ Boreaux, Carletti, S. & Vittot (2012) Com. Nonlin. Sci. Num. Sim., 17, 1725
  - ✓ Boreaux, Carletti, S., Papaphilippou & Vittot (2012) Int. J. Bif. Chaos, 22, 1250219

- **GALI**
  - ✓ S., Bountis & Antonopoulos (2007) Physica D, 231, 30
  - ✓ S., Bountis & Antonopoulos (2008) Eur. Phys. J. Sp. Top., 165, 5
  - ✓ Gerlach, Eggl & S. (2012) Int. J. Bif. Chaos, 22, 1250216
  - ✓ Manos, S. & Antonopoulos (2012) Int. J. Bif. Chaos, 22, 1250218
  - ✓ Manos, Bountis & S. (2013) J. Phys. A, 46, 254017

- **Reviews on SALI and GALI**
  - ✓ Bountis & S. (2012) 'Complex Hamiltonian Dynamics', Chapter 5, Springer Series in Synergetics
  - ✓ S. & Manos (2016) Lect. Notes Phys., 915, 129

Main References IV

- Lagrangian descriptors (LDs)
  - ✓ Madrid & Mancho (2009) Chaos, 19, 013111
  - ✓ Mendoza & Mancho (2010) Phys. Rev. Lett., 105, 038501
  - ✓ Mancho, Wiggins, Curbelo & Mendoza (2013) Commun. Nonlin. Sci. Num. Simul., 18, 3530
  - ✓ Lopesino, Balibrea, Wiggins & Mancho (2015) Commun. Nonlin. Sci. Num. Simul., 27, 40
  - ✓ Lopesino, Balibrea-Iniesta, García-Garrido, Wiggins & Mancho, (2017) Int. J. Bifurc. Chaos, 27, 1730001
  - ✓ Agaoglou, Aguilar-Sanjuan, García-Garrido, González-Montoya, Katsanikas, Krajňák, Naik & Wiggins (2020) 'Lagrangian descriptors: Discovery and quantification of phase space structure and transport', https://doi.org/10.5281/zenodo.3958985
  - ✓ Montes, Revuelta & Borondo (2021) Commun. Nonlin. Sci. Num. Simul., 102, 105860
  - ✓ Daquin, Pédenon-Orlanducci, Agaoglou, García-Sánchez & Mancho (2022) Physica D, 442, 133520

- Chaos diagnostics based on LDs
  - ✓ Hillebrand, Zimper, Ngapasare, Katsanikas, Wiggins & S. (2022) Chaos, 32, 123122
  - ✓ Zimper, Ngapasare, Hillebrand, Katsanikas, Wiggins & S. (2023) Physica D, 453, 133833

A …shameless promotion

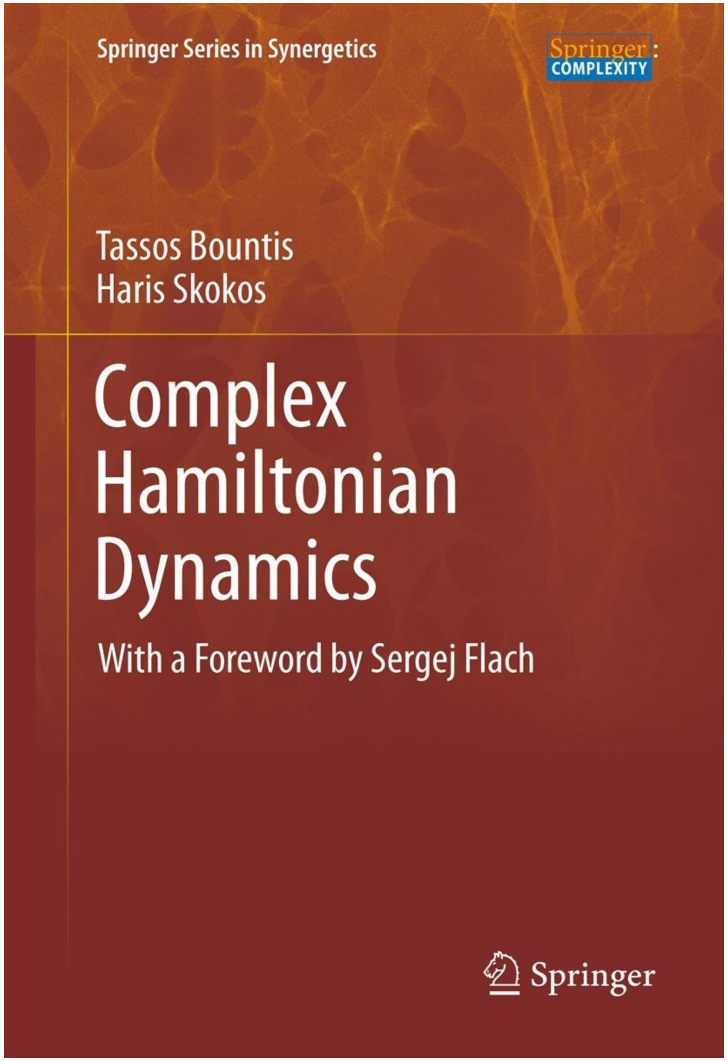

2012, Springer Series in Synergetics

Contents

Another …shameless promotion

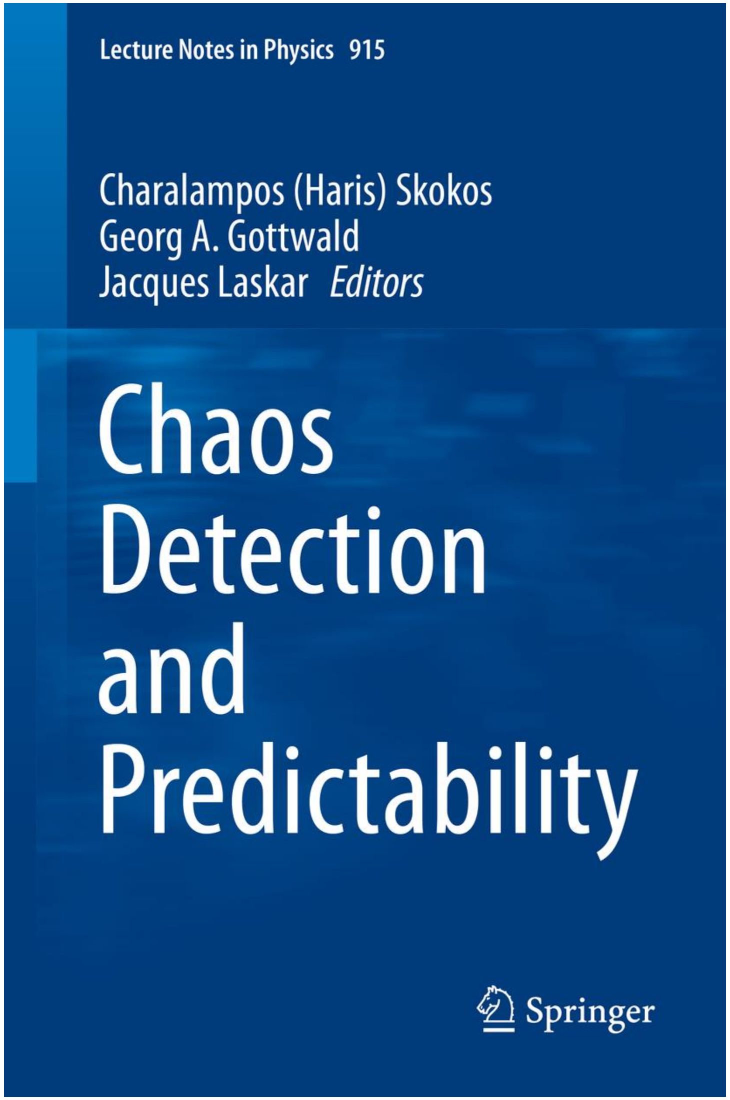

2016, Lect. Notes Phys., 915, Springer

Contents